Inhibitory CCK+ basket synapse defects in mouse models of dystroglycanopathy

Jennifer N. Jahncke[1,], Daniel S. Miller[1,], Milana Krush[1], Eric Schnell[2,3], and Kevin M. Wright[4,#]

[1] Neuroscience Graduate Program, Oregon Health & Science University, Portland, OR 97239, USA

[2] Operative Care Division, Portland VA Health Care System

[3] Anesthesiology and Perioperative Medicine, Oregon Health & Science University, Portland, OR 97239, USA

[4] Vollum Institute, Oregon Health & Science University, Portland, OR 97239, USA

[#] Correspondence to Kevin M Wright (wrighke@ohsu.edu). Vollum Institute, 3181 SW Sam Jackson Park Rd L474 Portland, OR 97239. (503)-494-6955

Keywords: dystroglycan, dystroglycanopathy, cannabinoid receptor, cholecystokinin, interneuron, synapse

Competing interests: The authors declare that they have no competing interests.

Acknowledgments
This work was funded by NIH Grants R01NS091027 (KMW), R01NS126247 (ES) CureCMD (KMW), F31NS120649 (JNJ), F31NS108522 (DSM), P30NS061800 (OHSU ALM), VA I01-BX004938 (ES), Department of Defense W81XWH-18-1-0598 (ES). The contents of this manuscript do not represent the views of the US Department of Veterans Affairs or the US government.

Author Contributions
J.N.J., D.S.M, E.S., and K.M.W. designed experiments. J.N.J, D.S.M., and M.K. performed experiments. J.N.J and D.S.M performed data analysis. J.N.J, D.S.M., and K.M.W. wrote the manuscript.

ABSTRACT

Dystroglycan (Dag1) is a transmembrane glycoprotein that links the extracellular matrix to the actin cytoskeleton. Mutations in *Dag1* or the genes required for its glycosylation result in dystroglycanopathy, a type of congenital muscular dystrophy characterized by a wide range of phenotypes including muscle weakness, brain defects, and cognitive impairment. We investigated interneuron (IN) development, synaptic function, and associated seizure susceptibility in multiple mouse models that reflect the wide phenotypic range of dystroglycanopathy neuropathology. Mice that model severe dystroglycanopathy due to forebrain deletion of *Dag1* or *Pomt2*, which is required for Dystroglycan glycosylation, show significant impairment of CCK^+/CB_1R^+ IN development. CCK^+/CB_1R^+ IN axons failed to properly target the somatodendritic compartment of pyramidal neurons in the hippocampus, resulting in synaptic defects and increased seizure susceptibility. Mice lacking the intracellular domain of Dystroglycan have milder defects in $CCK^+/CB1R^+$ IN axon targeting, but exhibit dramatic changes in inhibitory synaptic function, indicating a critical postsynaptic role of this domain. In contrast, CCK^+/CB_1R^+ IN synaptic function and seizure susceptibility was normal in mice that model mild dystroglycanopathy due to partially reduced Dystroglycan glycosylation. Collectively, these data show that inhibitory synaptic defects and elevated seizure susceptibility are hallmarks of severe dystroglycanopathy, and show that Dystroglycan plays an important role in organizing functional inhibitory synapse assembly.

INTRODUCTION

The formation of neural circuits is a multistep process involving proliferation, migration, axon guidance, maturation of neuronal subtypes, and establishment of functional synaptic connections between neurons. The cell adhesion molecule Dystroglycan is widely expressed in muscle and brain. Within the forebrain, Dystroglycan is expressed in neuroepithelial cells, pyramidal neurons, astrocytes, oligodendrocytes, and vascular endothelial cells where it plays important roles in the formation of basement membranes during early brain development (Colognato et al., 2007; Nguyen et al., 2014; Nickolls & Bönnemann, 2018; Tian et al., 1996; Zaccaria et al., 2001). At later developmental stages, Dystroglycan is present at multiple synapses, including at photoreceptor ribbon synapses in the retina (Omori et al., 2012; Orlandi et al., 2018), inhibitory synapses in the cerebellum (Briatore et al., 2010, 2020; Patrizi et al., 2008), and inhibitory synapses onto pyramidal neurons (Brünig et al., 2002; Lévi et al., 2002).

Dystroglycan is a central component of the dystrophin-glycoprotein complex (DGC) known primarily for its role in the etiology of neuromuscular diseases including Duchenne muscular dystrophy (DMD), limb-girdle muscular dystrophy (LGMD), and congenital muscular dystrophy (CMD). The gene encoding *Dystroglycan* (*Dag1*) yields two subunits, the extracellular alpha Dystroglycan (α-Dag1) and the transmembrane beta Dystroglycan (β-Dag1). These two subunits are non-covalently bound, allowing Dystroglycan to function as a link between extracellular ligands and cytoskeletal and signaling proteins (Ervasti & Campbell, 1991; Holt et al., 2000; Ibraghimov-Beskrovnaya et al., 1992; C. J. Moore & Winder, 2010). Extracellular α-Dag1 interacts with multiple

46 proteins in the nervous system through its extensive glycan chains (Jahncke & Wright,
47 2023). Mutations in any of the 19 genes involved in α-Dag1 glycosylation impair
48 Dystroglycan function through reduced ligand binding and leads to a class of congenital
49 muscular dystrophy termed dystroglycanopathy (Blaeser et al., 2013). Patients with
50 severe forms of dystroglycanopathy frequently present with structural brain
51 abnormalities and experience seizures and cognitive impairments (Barresi & Campbell,
52 2006; Muntoni et al., 2011; Taniguchi-Ikeda et al., 2016). Dystroglycanopathy patients
53 with moderate severity can exhibit cognitive impairments even in the absence of
54 identifiable brain malformations, suggesting that Dystroglycan functions at later stages
55 of neural circuit formation such as synapse formation and/or maintenance (Clement et
56 al., 2008; Godfrey et al., 2007).

57 The dramatic structural and anatomical phenotypes of global *Dag1* deletion in
58 mice has often precluded analysis of Dystroglycan's synaptic functions (Myshrall et al.,
59 2012; Satz et al., 2008, 2010). Recent studies show that when *Dag1* is selectively
60 deleted from postmitotic pyramidal neurons, neuronal migration and lamination is
61 normal, however CCK^+/CB_1R^+ interneurons (INs) fail to populate the forebrain or form
62 synapses in these mice (Früh et al., 2016; Miller & Wright, 2021). Furthermore,
63 conditional deletion of *Dag1* from cerebellar Purkinje neurons leads to impaired
64 inhibitory synaptic transmission and a reduction in the number of inhibitory synapses in
65 cerebellar cortex (Briatore et al., 2020). These studies establish a role for Dystroglycan
66 function at a subset of inhibitory synapses in the brain, but the critical features of
67 Dystroglycan necessary for these functions, and the relationship between inhibitory

68 synaptogenesis and neurological phenotypes in dystroglycanopathy, remains
69 undefined.
70 Here, we use multiple mouse models that recapitulate the full range of
71 dystroglycanopathy neuropathology to address several outstanding questions related to
72 the role of Dystroglycan at inhibitory synapses. We find that CCK^+/CB_1R^+ IN axon
73 targeting, synapse formation, and synapse function requires both glycosylation of α-
74 Dag1 and interactions through the intracellular domain of β-Dag1, and that defects in
75 synaptic structure and function is associated with increased seizure susceptibility in
76 mouse models of dystroglycanopathy.

77 **RESULTS**

78 **Characterizing Dystroglycan localization and glycosylation in multiple models of**
79 **dystroglycanopathy**

80 While conditional deletion of *Dag1* from pyramidal neurons causes a loss of
81 CCK^+/CB_1R^+ IN innervation in the forebrain, this has not been examined in
82 dystroglycanopathy relevant mouse models exhibiting more widespread loss of
83 functional Dystroglycan. We therefore generated five distinct mouse models; three to
84 provide mechanistic insight into Dystroglycan function and two of which model mild
85 dystroglycanopathy (schematized in **Fig. 1A**). Since complete loss of *Dag1* results in
86 early embryonic lethality in mice, we generated forebrain-specific conditional knockouts
87 by crossing $Emx1^{Cre}$ with *Dystroglycan* floxed mice ($Dag1^{F/F}$), to drive recombination in
88 neuroepithelial cells in the dorsal forebrain beginning at embryonic day 10.5 (E10.5)
89 (Gorski et al., 2002; Liang et al., 2012). We verified the recombination pattern of
90 $Emx1^{Cre}$ with the mCherry reporter $Rosa26^{Lox\text{-}STOP\text{-}Lox\text{-}H2B:mCherry}$. H2B:mCherry signal

91 was present in all excitatory neurons and astrocytes throughout the forebrain (**Fig. 1**
92 **Supp. 1A, B, D**) but not microglia or interneurons (**Fig. 1 Supp. 1C, E**).
93 To model loss of Dystroglycan glycosylation, *Emx1*^{Cre} was crossed with *Pomt2*$^{F/F}$
94 conditional mice to generate *Pomt2*^{cKOs}. Pomt2 (protein *O*-mannosyltransferase 2) is a
95 glycosyltransferase that functions in a heterocomplex with Pomt1 to add *O*-mannose at
96 the beginning of the Dystroglycan glycan chain (Manya et al., 2004). Without the initial
97 *O*-mannose, no additional sugar moieties can be added to the glycan chain, resulting in
98 near complete loss of Dystroglycan glycosylation. This is lethal embryonically in a global
99 *Pomt2* knockout, however *Emx1*^{Cre};*Pomt2*^{cKO} mice are viable and survive into adulthood
100 (Hu et al., 2016; Reeuwijk et al., 2005; Yanagisawa et al., 2007).
101 In addition to binding extracellular ligands, Dystroglycan binds cytoskeletal
102 proteins and signals through the intracellular tail of its β-subunit. To determine whether
103 the intracellular domain of Dystroglycan is required for synaptic development and/or
104 function, we examined mice in which one copy of *Dag1* was deleted, and the other copy
105 lacks the intracellular domain of β-Dag1 (*Dag1*$^{cyto/-}$). These mice develop muscular
106 dystrophy but show normal neuronal migration and axon guidance in regions throughout
107 the central nervous system where Dystroglycan glycosylation is required (Lindenmaier
108 et al., 2019; Satz et al., 2009, 2010).
109 To model mild forms of dystroglycanopathy, we examined mice expressing
110 missense mutations in *B4gat1 (*β-1,4-glucuronyltransferase, *B4gat1*^{M155T}) and *Fkrp*
111 (fukutin related protein, *Fkrp*^{P448L}), two genes required for Dystroglycan glycosylation.
112 *B4gat1*^{M155T} mice were initially identified in a forward genetic screen and develop mild
113 muscular dystrophy and have diminished ligand binding capacity due to reduced

114 Dystroglycan glycosylation (Wright et al., 2012). The *Fkrp*^{P448L} missense mutation
115 models a mutation found in a patient with dystroglycanopathy (Brockington et al., 2001).
116 In mice, the *Fkrp*^{P448L} mutation leads to reduced glycosylation and mild muscular
117 dystrophy, but no gross brain or eye malformations (Blaeser et al., 2013). While it is
118 possible that *Pomt2*, *B4gat1*, and *Fkrp* could play a role in the glycosylation of proteins
119 other than Dystroglycan, the identity of these proteins has not been described in
120 neurons to date and we did not observe any emergent phenotypes that have not been
121 observed in *Dag1* mutants (Gerin et al., 2016; Larsen, Narimatsu, Joshi, Siukstaite, et
122 al., 2017; Larsen, Narimatsu, Joshi, Yang, et al., 2017; Willer et al., 2014).
123 We first examined the pattern of Dystroglycan localization in pyramidal neurons
124 in CA1 of hippocampus in each of the five models by immunostaining adult (P30) mice
125 with the IIH6 antibody, which detects the terminal matriglycan repeats on the glycan
126 chain on α-Dag1 (Sheikh et al., 2022; Yoshida-Moriguchi & Campbell, 2015). In wild-
127 type (WT) mice, punctate IIH6 immunoreactivity was evident in the somatic and
128 perisomatic compartment of CA1 pyramidal neurons (**Fig. 1A**). Immunoreactivity was
129 also present in blood vessels, where *Dag1* is also expressed (Durbeej et al., 1998;
130 Zaccaria et al., 2001). Neuronal immunoreactivity was undetectable in
131 *Emx1*^{Cre}*;Dag1*^{cKOs} and *Emx1*^{Cre}*;Pomt2*^{cKOs}, whereas blood vessel expression was
132 maintained, illustrating the specificity of the conditional deletion (**Fig. 1A**). Punctate
133 perisomatic IIH6 immunoreactivity was present in *Dag1*$^{cyto/-}$, *B4gat1*$^{M155T/M155T}$, and
134 *Fkrp*$^{P448L/P448L}$ mice (**Fig. 1A**). To assess Dystroglycan localization in *Emx1*^{Cre}*;Pomt2*^{cKOs}
135 we used an antibody that recognizes the intracellular C-terminus of β-Dag1. Although
136 immunoreactivity for β-Dag1 was present and elevated above *Emx1*^{Cre}*;Dag1*^{cKO} or

137 *Dag1*$^{cyto/-}$ levels, Dag1 localization did not appear punctate in *Emx1*^{Cre}*;Pomt2*^{cKOs} (**Fig. 1**
138 **Supp. 2A**). This apparent difference implies that Dag1 glycosylation, and by extension
139 the extracellular interactions that matriglycan mediates, is required for proper Dag1
140 synaptic localization.

141 We next prepared WGA-enriched lysate from neonatal (P0) forebrain and
142 immunoblotted for (1) IIH6, to quantify the degree of α-Dag1 glycosylation and (2) β-
143 Dag1, to measure total Dystroglycan protein levels (**Fig. 1B**). Dag1 glycosylation was
144 significantly reduced in *Emx1*^{Cre}*;Dag1*^{cKOs}, *Emx1*^{Cre}*;Pomt2*^{cKOs}, *Dag1*$^{cyto/-}$,
145 *B4gat1*$^{M155T/M155T}$, and *Fkrp*$^{P448L/P448L}$ mice; however, the reduction in *Fkrp*$^{P448L/P448L}$ mice
146 was less severe than the other models (**Fig. 1C**). The reduction in glycosylation
147 observed in the *Dag1*$^{cyto/-}$ mice is surprising given that the mutation is restricted to the
148 intracellular domain. *Dystroglycan* heterozygotes (*Dag1*$^{+/-}$) show no reduction in IIH6
149 levels compared to wild-types (data not shown), so the reduction in *Dag1*$^{cyto/-}$ mice can
150 be presumed to be due to the intracellular deletion. It is possible that the intracellular
151 domain is required for the trafficking of Dystroglycan through the endoplasmic reticulum
152 and/or Golgi apparatus, where Dystroglycan undergoes glycosylation, however
153 additional work is needed to verify this. As expected, β-Dag1 immunoblotting was
154 significantly reduced in *Emx*^{Cre}*;Dag1*^{cKOs} and absent in *Dag1*$^{cyto/-}$ mice but normal in the
155 glycosylation mutants (**Fig. 1D**). The residual β-Dag1 in *Emx1*^{Cre}*;Dag1*^{cKO} brain is likely
156 due to *Dag1* expression in unrecombined cells, such as blood vessels, as well as
157 unrecombined tissue that remained after the forebrain dissection.

158 We next examined Dag1 protein levels during synaptogenesis using WGA-
159 enriched lysate from P21-P30 hippocampus. As expected, Dag1 glycosylation assessed

160 by IIH6 immunoblotting was severely reduced in *Emx1^{Cre};Dag1^{cKOs}* and
161 *Emx1^{Cre};Pomt2^{cKOs}* but normal in *Dag1$^{cyto/-}$* mice (**Fig. 1 Supp. 2B-C**). Immunoblotting
162 for β-Dag1 showed a significant reduction in *Emx1^{Cre};Dag1^{cKOs}* and *Dag1$^{cyto/-}$* mutants
163 but normal levels in *Emx1^{Cre};Pomt2^{cKOs}* (**Fig. 1 Supp. 2B, D**). Although localization of
164 Dag1 was not punctate in *Emx1^{Cre};Pomt2^{cKOs}* (**Fig. 1 Supp. 2A**), the overall level of β-
165 Dag1 was normal by WGA-enrichment, which enriches for proteins in the plasma
166 membrane (**Fig. 1 Supp. 2B, D**). It therefore remains possible that Dag1 still trafficks to
167 the cell surface in *Emx1^{Cre};Pomt2^{cKOs}* but fails to contact presynaptic axons and
168 therefore does not permit synaptogenesis.
169
170 **Dystroglycan is required for cortical neuron migration in a glycosylation-**
171 **dependent manner**
172 In neocortex, *Dag1* expression in radial glia is required for proper migration of
173 neurons, with *Dag1* conditional deletion from neuroepithelial cells or radial glia resulting
174 in Type II lissencephaly (S. A. Moore et al., 2002; Pawlisz & Feng, 2011; Satz et al.,
175 2008, 2010). This requires proper Dystroglycan glycosylation, but not its expression in
176 neurons (Chan et al., 2010; Holzfeind et al., 2002; Hu et al., 2011; Wright et al., 2012).
177 To compare cortical migration across our five models of dystroglycanopathy, we
178 performed immunostaining for the upper layer marker Cux1 (layers II/III-IV) and the
179 deep layer marker Tbr1 (layers III, VI) in P30 somatosensory cortex (**Fig. 2A-B**).
180 *Emx1^{Cre};Dag1^{cKOs}* and *Emx1^{Cre};Pomt2^{cKOs}* showed complete cortical dyslamination with
181 100% penetrance, whereas the cytoplasmic (*Dag1$^{cyto/-}$*) deletion mutants appeared
182 normal (**Fig. 2C-D**). *B4gat1$^{M155T/M155T}$* missense mutants showed a migration phenotype

183 only at the cortical midline, while *Fkrp*$^{P448L/P448L}$ missense mutants did not show any
184 cortical migration phenotype (**Fig. 2 C-D, Fig. 2 Supp. 1A**). These results indicate that
185 cortical migration depends on Dystroglycan glycosylation but does not require its
186 cytoplasmic domain. Furthermore, taken with the data in **Fig. 1B-D**, they illustrate that
187 the severity of the cortical migration phenotype scales with the degree of Dystroglycan
188 hypoglycosylation; *Emx1*^{Cre}*;Dag1*^{cKOs} and *Emx1*^{Cre}*;Pomt2*^{cKOs} model a severe form of
189 dystroglycanopathy (Walker-Warburg Syndrome, Muscle-Eye-Brain disease) and
190 *B4gat1*$^{M155T/M155T}$ and *Fkrp*$^{P448L/P448L}$ mutants modeling a milder form of the disease.
191 To further assess the impact of our functional domain mutations, we assessed
192 Laminin localization, the canonical interacting partner of Dystroglycan in the
193 extracellular matrix (ECM), in adult neocortex (Ibraghimov-Beskrovnaya et al., 1992).
194 Under WT conditions, Laminin immunoreactivity was evident at the pial surface where
195 Laminin and Dystroglycan interact at the interface between radial glial endfeet and the
196 cortical basement membrane (Satz et al., 2010). Laminin was also present in blood
197 vessels, where Dystroglycan-expressing perivascular astrocytes contribute to the
198 maintenance of water homeostasis (Menezes et al., 2014). In *Emx1*^{Cre}*;Dag1*^{cKO} cortex,
199 Laminin immunoreactivity at the pial surface was patchy and vascular Laminin showed
200 evidence of the neuronal migration phenotype described in **Fig. 2** (**Fig. 2 Supp. 2A**).
201 Laminin immunoreactivity in *Emx1*^{Cre}*;Pomt2*^{cKO} cortex similarly showed a patchy
202 appearance, albeit less severe than *Emx1*^{Cre}*;Dag1*^{cKOs}, along with the evident cortical
203 migration phenotype (**Fig. 2 Supp. 2B**). *Dag1*$^{cyto/-}$ mutants, on the other hand, exhibited
204 normal Laminin immunoreactivity both at the pial surface and with regards to vascular
205 organization (**Fig. 2 Supp. 2C**).

206

207 **Perisomatic CCK$^+$/CB$_1$R$^+$ interneuron targeting requires Dystroglycan in a non-**

208 **cell autonomous manner**

209 CCK$^+$/CB$_1$R$^+$ IN innervation is largely absent from the cortex and hippocampus

210 when *Dag1* is deleted selectively from pyramidal neurons using *NEX^{Cre}* (Früh et al.,

211 2016; Miller & Wright, 2021). However, the development and function of CCK$^+$/CB$_1$R$^+$

212 INs has not been examined in mouse models that more broadly lack *Dag1* throughout

213 the central nervous system (CNS) and thus more accurately reflect the neuropathology

214 of dystroglycanopathy. We focused our analysis on region CA1 of the hippocampus, as

215 its overall architecture is grossly unaffected in each of our mouse models. Both

216 *Emx1^{Cre};Dag1^{cKO}* and *Emx1^{Cre};Pomt2^{cKO}* mice exhibited a mild granule cell migration

217 phenotype in dentate gyrus (**Fig. 3A**, yellow arrows), however CA1-CA3 showed normal

218 pyramidal neuron organization.

219 In WT control mice, CCK$^+$/CB$_1$R$^+$ IN axon terminals were abundant throughout

220 the hippocampus, with their highest innervation density in the CA1 pyramidal cell body

221 layer (*stratum pyramidale*, SP) where they form characteristic basket synapses onto

222 pyramidal neurons (**Fig. 3A-C**, **Fig. 3 Supp. 1A**). In *Emx1^{Cre};Dag1^{cKO}* mice,

223 CCK$^+$/CB$_1$R$^+$ axons were present but failed to target the pyramidal cell layer (**Fig. 3A-C**,

224 **Fig. 3 Supp. 1A**), a surprising difference from the phenotype observed in

225 *NEX^{Cre};Dag1^{cKO}* mice which lack CCK$^+$/CB1R$^+$ IN innervation entirely (Früh et al., 2016;

226 Miller & Wright, 2021) (**Fig. 3 Supp. 1C**). To confirm the CCK$^+$/CB1R$^+$ IN innervation

227 pattern in the context of widespread *Dag1* deletion, we generated *Nestin^{Cre};Dag1^{cKO}*

228 mice. *Nestin^{Cre}*, similar to *Emx1^{Cre}*, drives *Cre* recombination in forebrain progenitors,

229 however *Emx1*^{Cre} recombination begins around E10.5 and *Nestin*^{Cre} recombination
230 begins around E11.5 (Liang et al., 2012; Tronche et al., 1999). *Nestin*^{Cre}*;Dag1*^{cKOs}
231 showed the same CCK^{+}/CB1R^{+} axon targeting phenotype as *Emx1*^{Cre}*;Dag1*^{cKOs} (**Fig. 3**
232 **Supp. 1B**), further suggesting that the observed *Emx1*^{Cre}*;Dag1*^{cKO} phenotype faithfully
233 models dystroglycanopathy neuropathology.
234 It was previously reported that the lack of CCK^{+}/CB1R^{+} IN innervation of CA1
235 pyramidal neurons observed in *NEX*^{Cre}*;Dag1*^{cKOs} was accompanied by reduced
236 numbers of CCK^{+}/CB1R^{+} INs (Miller & Wright, 2021). We therefore sought to quantify
237 CCK^{+}/CB1R^{+} IN cell density in *Emx1*^{Cre}*;Dag1*^{cKOs} using both NECAB1 and NECAB2
238 antibodies (Miczán et al., 2021). As NECAB1 is expressed by both CCK^{+}/CB$_{1}$R^{+} INs and
239 PV^{+} INs, we performed immunolabeling for both NECAB1 and PV and quantified the
240 density of NECAB1^{+};PV^{-} cell bodies in CA1, finding no difference between
241 *Emx1*^{Cre}*;Dag1*^{Ctrls} and *Emx1*^{Cre}*;Dag1*^{cKOs} (**Fig. 3 Supp. 2A-B**). To confirm this, we also
242 quantified the density of NECAB2^{+} cell bodies in CA1, again finding no difference
243 between genotypes (**Fig. 3 Supp. 2C, E**). Thus, the observed change in CCK^{+}/CB$_{1}$R^{+} IN
244 axon targeting of CA1 pyramidal cells is not due to a reduction in cell numbers, but
245 rather a failure to innervate the appropriate compartment.
246 *Emx1*^{Cre}*;Pomt2*^{cKO} mice fully phenocopied the aberrant *Emx1*^{Cre}*;Dag1*^{cKO} CB$_{1}$R^{+}
247 immunoreactivity pattern (**Fig. 3A-C**), demonstrating that proper CCK^{+}/CB$_{1}$R^{+} IN basket
248 axon targeting requires Dystroglycan glycosylation. Both the *B4gat1* and *Fkrp* mutants
249 showed a normal distribution of CB$_{1}$R^{+} axon targeting to the somatodendritic
250 compartment of CA1 neurons, but with reduced CB$_{1}$R intensity in SP (**Fig. 3A-C**). The
251 cytoplasmic domain of Dystroglycan also plays a role in the appropriate targeting of

252 CB_1R immunoreactive axons, as the distribution of axons was perturbed in the *Dag1*$^{cyto/-}$
253 mutants, though with an intermediate phenotype in which the upper portion of SP
254 appeared normal while the lower portion of SP showed loss of selective CB_1R^+ axon
255 targeting (**Fig. 3A-C**).

256 Due to the axonal targeting defect in the CCK^+/CB_1R^+ IN population, we next
257 examined the parvalbumin (PV) population of interneurons in the hippocampus, as
258 these cells also form perisomatic basket cell synapses on to CA1 pyramidal cells. There
259 was no significant difference in the number of PV^+ INs in CA1 of *Emx1*^{Cre}*;Dag1*^{cKO} mice
260 and littermate controls (**Fig. 3 Supp. 2D, F**). Furthermore, the distribution of PV^+ IN
261 axons showed normal targeting to SP in all mouse models (**Fig. 3 Supp. 3A-B**),
262 indicating that the axon targeting phenotype is specific to the CCK^+/CB_1R^+ IN
263 population. Interestingly, *Emx1*^{Cre}*;Dag1*^{cKO} mice exhibited a slight increase in PV
264 intensity in SP, perhaps indicating that there is a degree of compensation (**Fig. 3 Supp.**
265 **3A-B**).

266 Notably, CB_1R expression was also abnormal in brain regions outside of the
267 hippocampus. In somatosensory cortex, CB_1R immunostaining reflected the
268 dyslamination phenotype in both the *Emx1*^{Cre}*;Dag1*^{cKO} and *Emx1*^{Cre}*;Pomt2*^{cKO} mice
269 throughout neocortex and the *B4gat1*$^{M155T/M155T}$ mice at midline, while it appeared
270 normal in cortex of *Dag1*$^{cyto/-}$ and *Fkrp*$^{P448L/P448L}$ mice (**Fig. 3 Supp. 4A**). CB_1R staining
271 was also reduced and disorganized in the basolateral amygdala (BLA) in
272 *Emx1*^{Cre}*;Dag1*^{cKO} and *Emx1*^{Cre}*;Pomt2*^{cKO} mice (**Fig. 3 Supp. 4B**). Interestingly, CB_1R
273 immunostaining in the inner molecular layer (IML) of dentate gyrus appears normal in all
274 mutants (**Fig. 3A**). In the IML, CB_1R is present in excitatory mossy cell axons targeting

275 dentate granule cells whereas in both cortex and amygdala CB_1R expression is
276 restricted to GABAergic interneurons (Földy et al., 2006; Katona et al., 2001; Monory et
277 al., 2015). Therefore, glycosylated Dystroglycan instructs the development of inhibitory
278 CB_1R^+ interneuron populations in multiple brain regions.
279

280 **Dystroglycan is required for CCK^+/CB_1R^+ interneuron axon targeting during early**
281 **postnatal development**

282 During early postnatal development, CCK^+/CB_1R^+ IN axons undergo a dramatic
283 laminar rearrangement, progressing from more distal localization amongst pyramidal
284 cell dendrites, to eventually target pyramidal neuron cell bodies in the hippocampus
285 (Miller & Wright, 2021; Morozov et al., 2009; Morozov & Freund, 2003a, 2003b). We
286 examined the developmental time course of CCK^+/CB_1R^+ IN axon targeting in our
287 *Emx1^{Cre};Dag1^{cKO}* mice beginning at P5, when the axons are first readily identifiable
288 (Berghuis et al., 2007; Eggan et al., 2010; Mulder et al., 2008; Vitalis et al., 2008). At P5
289 in control *Emx1^{Cre};Dag1^{Ctrl}* mice, CCK^+/CB_1R^+ axons were initially concentrated in the
290 *stratum radiatum* (SR) of the hippocampus (**Fig. 4A-C**). Between P10 and P30, the
291 CCK^+/CB_1R^+ axons underwent developmental reorganization, with reduced innervation
292 of SR coinciding with a progressive increase in innervation of SP. In contrast, overall
293 CCK^+/CB_1R^+ innervation was initially reduced in the hippocampus of mutant
294 *Emx1^{Cre};Dag1^{cKO}* mice at P5, and these axons failed to undergo laminar reorganization
295 as they developed (**Fig. 4A-C**). By P30, after IN synapse formation and targeting are
296 largely complete in control mice, the density of CCK^+/CB_1R^+ axons in *Emx1^{Cre};Dag1^{cKO}*
297 mice was uniform across all hippocampal lamina (**Fig. 4A-C**). Therefore, Dystroglycan

298 plays a critical developmental role during the first two postnatal weeks, for the proper
299 laminar distribution and perisomatic targeting of CCK^+/CB_1R^+ IN axons in the
300 hippocampus.
301
302 **CCK^+/CB_1R^+ IN synapse formation requires postsynaptic glycosylated**
303 **Dystroglycan**
304 Given the perturbed distribution of CCK^+/CB_1R^+ IN axons in the hippocampus,
305 we next wanted to determine whether the remaining CCK^+/CB_1R^+ IN axons were
306 capable of forming synapses in dystroglycanopathy models. Using VGAT as a marker of
307 inhibitory presynaptic terminals, we saw no difference in total VGAT puncta density in
308 SP in any of the mouse models, indicating that the total number of inhibitory synapses is
309 normal (**Fig. 5B-D**). Immunostaining for CB_1R showed a significant decrease in CB_1R in
310 SP of *Emx1*^{Cre}*;Dag1*^{cKO}, *Emx1*^{Cre}*;Pomt2*^{cKO}, *B4gat1*$^{M155T/M155T}$, and *Fkrp*$^{P448L/P448L}$
311 mutants, but not *Dag1*$^{cyto/-}$ mutants (**Fig. 5E**). This suggests that the difference in CB_1R^+
312 axon distribution described in SP of *Dag1*$^{cyto/-}$ mutants in **Fig. 3A-C** likely reflects a
313 change in CCK^+/CB_1R^+ IN axon targeting but not synapse formation, whereas
314 *Emx1*^{Cre}*;Dag1*^{cKO} and all three glycosylation mutants exhibit a reduction in CCK^+/CB_1R^+
315 IN axon targeting and synapse number in SP. It should be noted that the data in **Fig.**
316 **3A-C** reflects axonal CB_1R intensity across all hippocampal layers, whereas the
317 quantification in **Fig. 5E** reflects the density of axonal swellings within SP. These data
318 therefore suggest that there is an overall reduction in CB_1R intensity in SP of *Dag1*$^{cyto/-}$
319 mutants that does not influence the number of CB_1R^+ axonal swellings. In contrast to
320 CCK^+/CB_1R^+ INs, the PV^+ population of basket interneurons showed no change in

321 puncta density in SP in any of the models (**Fig. 5 Supp. 2A-E**; analysis of VGAT, CB_1R,
322 and PV densities in SO and SR included in **Fig. 5 Supp. 1A-B** and **Fig. 5 Supp. 3A**.)
323 To better approximate the extent of basket synapse formation, we quantified the
324 co-localization between VGAT and CB_1R or PV. In SP, the percent of CB_1R puncta co-
325 localized with VGAT was reduced in the same models that showed a reduction in CB_1R
326 density (*Emx1*^{Cre}*;Dag1*^{cKO}, *Emx1*^{Cre}*;Pomt2*^{cKO}, *B4gat1*$^{M155T/M155T}$, and *Fkrp*$^{P448L/P448L}$
327 mutants) but not *Dag1*$^{cyto/-}$ mutants (**Fig. 5C, F**), suggesting that CCK^+/CB_1R^+ INs
328 require postsynaptic glycosylated Dystroglycan in order to form synapses whereas the
329 cytoplasmic domain is required for axon targeting but not synapse formation.
330 Interestingly, the percent of PV co-localized with VGAT increased in the SP of
331 *Emx1*^{Cre}*;Dag1*^{cKOs} and *Emx1*^{Cre}*;Pomt2*^{cKOs} mice, with no change in any of the other
332 models (**Fig. 5 Supp. 2C, E**; analysis of co-localization in SO and SR included in **Fig. 5**
333 **Supp. 1C**, **Fig. 5 Supp. 3B**). It is possible that the reduction in inhibitory $CCK^+/CB1R^+$
334 synapses prompts homeostatic compensation through an increase in PV^+ synapses.
335 Alternatively, this may reflect competition between CCK^+/CB_1R^+ and PV^+ INs for
336 physical space on the perisomatic region of pyramidal cells, with the decrease in
337 CCK^+/CB_1R^+ synapses in *Emx1*^{Cre}*;Dag1*^{cKOs} and *Emx1*^{Cre}*;Pomt2*^{cKOs} allowing additional
338 PV^+ IN synapses to form.
339
340 **CCK^+/CB_1R^+ interneuron basket synapse function is dependent on Dystroglycan**
341 **function**
342 Perisomatic inhibitory basket cell synapses powerfully control activity in the
343 hippocampal circuit (Freund & Katona, 2007). Previous studies in *NEX*^{Cre}*;Dag1*^{cKO} mice,

344 in which CCK^+/CB_1R^+ INs are absent, demonstrated reduced inhibitory synaptic function
345 (Früh et al., 2016). In the current study, however, CCK^+/CB_1R^+ INs are present but
346 mistargeted. Thus, we wanted to determine whether with the changes in CCK^+/CB_1R^+
347 basket synapse localization in our mouse models were associated with altered inhibitory
348 synaptic function. CCK^+/CB_1R^+ IN basket cells can be selectively activated by
349 muscarinic receptor activation, which increases the rate of spontaneous inhibitory post-
350 synaptic currents (sIPSCs) in nearby pyramidal cells (Früh et al., 2016; Nagode et al.,
351 2014). Thus, to assay function at CCK^+/CB_1R^+ IN synapses, we performed whole cell
352 patch clamp electrophysiology from CA1 pyramidal neurons in slices from control and
353 mutant mice. After recording 5 minutes of baseline sIPSCs, the cholinergic receptor
354 agonist Carbachol (CCh) was added to the bath and an additional 5 minutes of sIPSCs
355 were recorded. While both *Emx1*^{Cre}*;Dag1*^{Ctrl} and *Emx1*^{Cre}*;Dag1*^{cKO} cells displayed a
356 CCh-mediated change in sIPSC frequency, this response was dramatically attenuated
357 in *Emx1*^{Cre}*;Dag1*^{cKOs} mice compared to *Emx1*^{Cre}*;Dag1*^{Ctrl} mice (**Fig. 6A-C**). Furthermore,
358 in *Emx1*^{Cre}*;Dag1*^{Ctrls}, 19/21 cells (90.5%) responded to CCh application (defined as a
359 >20% increase in sIPSC frequency), whereas only 13/22 cells (59.1%) responded in
360 *Emx1*^{Cre}*;Dag1*^{cKOs} (**Fig. 6 Supp. 1B**). Proper Dystroglycan glycosylation was also
361 required for CCK^+/CB_1R^+ IN synapse function, as *Emx1*^{Cre}*;Pomt2*^{cKO} mice exhibited the
362 same phenotype as *Emx1*^{Cre}*;Dag1*^{cKOs}: a reduced response to CCh overall, and a
363 reduced proportion of responsive cells (**Fig. 6A-C**, **Fig. 6 Supp. 1B**). CCh also
364 increased the mean sIPSC amplitude in each of the controls (**Fig. 6 Supp. 1A**), which
365 may reflect an increased contribution of larger-amplitude action potential-mediated
366 perisomatic events elicited by CCh (Früh et al., 2016; Nagode et al., 2014). Consistent

367 with the decreased function of CCK^+/CB_1R^+ IN synapses, a CCh-mediated change in
368 sIPSC amplitude was also absent in each of these models (**Fig. 6 Supp. 1A**). Together,
369 these data indicate that the altered perisomatic CCK^+/CB_1R^+ IN synaptic localization in
370 CA1 is associated with a functional deficit in synaptic signaling.

371 *Dag1*$^{cyto/-}$ mutants also had a dramatically attenuated sIPSC response to CCh
372 compared to WT controls (**Fig. 6C)**. Notably, even baseline sIPSC frequency was
373 reduced in *Dag1*$^{cyto/-}$ mutants (2.27±1.70 Hz) compared to WT controls (4.46±2.04 Hz, p
374 = 0.002), whereas baseline sIPSC frequencies appeared normal in all other mutants
375 when compared to their respective controls. Together with the finding that these
376 mutants contain a normal number of CCK^+/CB_1R^+ basket synapses (as measured using
377 immunohistochemistry; **Fig. 5A-D**), these results indicate that the cytoplasmic domain of
378 Dystroglycan may play a critical role in mediating the assembly of functional
379 postsynaptic signaling/receptor complexes at these synapses.

380 Neither of the more mildly hypoglycosylated mutants (*B4gat1*$^{M155T/M155T}$,
381 *Fkrp*$^{P448L/P448L}$) were different from their respective littermate controls in terms of the
382 magnitude of the CCh effect on sIPSC frequency (**Fig. 6C**), although the *B4gat1*^{WT} mice
383 appeared to possess a reduced effect of CCh compared to other control conditions (**Fig.
384 6A-C**). The *B4gat1* line is of a mixed genetic background, which could possibly explain
385 the difference in CCh response. This finding is of unclear significance and may have
386 obscured potential differences. Importantly, however, the marked functional synaptic
387 differences observed between the *Emx1*^{Cre}*;Pomt2*^{cKO}, *Emx1*^{Cre}*;Dag1*^{cKO} and *Dag1*$^{cyto/-}$
388 mice when compared with each of their respective controls described above was not
389 seen in either of these phenotypically milder mutants.

390 Together, these results suggest that Dystroglycan is required for the function of
391 CCK^+/CB_1R^+ IN perisomatic basket synapses in a glycosylation-dependent manner, as
392 evidenced by the *Emx1*^{Cre}*;Dag1*^{cKO} and *Emx1*^{Cre}*;Pomt2*^{cKO} synaptic phenotypes, and
393 that the intracellular domain of Dystroglycan is also required for normal CCK^+/CB_1R^+ IN
394 basket synapse function. However, we cannot rule out the possibility that CCK^+/CB_1R^+
395 INs are simply less responsive to CCh in the mutants, as we lack the tools to identify
396 CCK^+/CB1R$^+$ INs in live tissue for targeted recordings. In contrast, *B4gat1*$^{M155T/M155T}$ and
397 *Fkrp*$^{P448L/P448L}$ hypomorphic mutants both appear to retain sufficient Dystroglycan
398 glycosylation to maintain normal synapse function.
399
400 **Increased seizure susceptibility in models of dystroglycanopathy**
401 Human patients with dystroglycanopathy have an increased risk of seizures and
402 epilepsy (Dhaibani et al., 2018; Di Rosa et al., 2011; Raphael et al., 2014; Yang et al.,
403 2022), however the underlying cause has yet to be determined. The observed defects in
404 inhibitory basket synapse function suggest that alterations in neuronal circuit inhibition
405 could potentially predispose mutant mice to seizures. To test whether mouse models of
406 dystroglycanopathy exhibit a reduced seizure threshold, we exposed mice to the volatile
407 chemoconvulsant flurothyl and measured the latency to generalized tonic-clonic seizure
408 (TCS) (Egawa et al., 2021).
409 The latency to TCS was significantly faster in *Emx1*^{Cre}*;Dag1*^{cKO} mice than their
410 littermate controls (a 40.9% reduction on average, **Fig. 7A**), with no difference in
411 seizure latency between sexes in either group (**Fig. 7 Supp. 1C**). *Emx1*^{Cre}*;Pomt2*^{cKOs}
412 and *Dag1*$^{cyto/-}$ mutants also had a significantly shorter latency to TCS than littermate

413 controls (42.9% and 33.6% reductions, respectively; **Fig. 7A**), indicating that the
414 mechanism underlying Dystroglycan's role in seizure susceptibility requires both
415 extracellular glycosylation and intracellular interactions. *B4gat1*$^{M155T/M155T}$ mutants
416 showed a small but significant reduction (16%) in seizure latency, despite exhibiting no
417 detectable functional deficit by electrophysiology (**Fig. 6A-C**, **Fig. 7A**). Finally,
418 *Fkrp*$^{P448L/P448L}$ mutants showed no significant change in seizure susceptibility (**Fig. 7A**).
419 Thus, the reduction in seizure latency reflects the severity of the synaptic phenotypes
420 across the various models of dystroglycanopathy. These results demonstrate that
421 disruptions in Dystroglycan function, including both its extracellular glycosylation and
422 intracellular interactions, increase sensitivity to seizures.
423

424 **DISCUSSION**

425 Recent work identified a key role for neuronal Dystroglycan in the establishment
426 and function of CCK$^+$/CB$_1$R$^+$ inhibitory synapses in the forebrain (Früh et al., 2016;
427 Miller & Wright, 2021). Deletion of *Dag1* selectively from pyramidal neurons
428 (*NEX*^{Cre}*;Dag1*^{cKO}) led to a near complete loss of CCK$^+$/CB$_1$R$^+$ INs during the first few
429 postnatal weeks. In this study, we sought to better understand how CCK$^+$/CB$_1$R$^+$ IN
430 synapse formation is affected in mouse models that more accurately reflect
431 dystroglycanopathy, in which Dystroglycan function is more broadly affected throughout
432 the CNS (**Figs. 1**, **2**). Using a model that deletes *Dag1* throughout the developing
433 forebrain (*Emx1*^{Cre}*;Dag1*^{cKO}) we found that CCK$^+$/CB$_1$R$^+$ INs were present, but the
434 laminar organization of their axon terminals and their ability to form functional basket
435 synapses onto pyramidal neuron cell bodies in the hippocampus was impaired (**Figs. 3-**

436 **6**). The inability of CCK^+/CB_1R^+axon terminals to concentrate in the CA1-3 cell body
437 layer began to manifest during the first postnatal week, when dynamic changes in
438 laminar innervation by CCK^+/CB_1R^+ axons normally occur (**Fig. 4**). Furthermore, these
439 mice were found to exhibit a reduced seizure threshold compared to controls, showing
440 for the first time that mouse models of dystroglycanopathy are vulnerable to seizures
441 (**Fig. 7**). Because *Emx1*^{Cre} (and *Nestin*^{Cre}) conditional deletion of *Dag1* or *Pomt2* leads
442 to widespread loss of functional Dystroglycan in the forebrain in contrast with the
443 previously studied *NEX*^{Cre} conditional deletion, which targets pyramidal neurons, these
444 models more accurately model dystroglycanopathy.
445 We found that CCK^+/CB_1R^+ IN synapse formation and function are dependent on
446 proper Dystroglycan glycosylation and appear to correlate with the degree of
447 hypoglycosylation in different mutants. Complete reduction of glycosylation in
448 *Emx1*^{Cre}*;Pomt2*^{cKO} mutants caused the same phenotypes seen in Dystroglycan
449 conditional knockouts (*Emx1*^{Cre}*;Dag1*^{cKO}) (**Figs. 1-3, 5-6**), possibly due to the
450 mislocalization of Dystroglycan. The finding that glycosylation is required for
451 Dystroglycan synaptic localization in hippocampal pyramidal cells is similar to a
452 previous finding in retinal photoreceptors in the context of *Pomt1* conditional deletion
453 (Rubio-Fernández et al., 2018). In contrast, when *Fktn* deletion is induced in myotubes
454 β-Dystroglycan localization is unchanged, suggesting that this phenomenon is unique to
455 synaptic Dystroglycan (Beedle et al., 2012). One interpretation is that without
456 matriglycan present to mediate interaction with presynaptic cells, Dystroglycan is no
457 longer concentrated at synaptic sites, implicating it as a synaptic organizer. However,
458 the miswiring of the CCK^+/CB_1R^+ axons could also reduce the likelihood of postsynaptic

459 Dystroglycan encountering a presynaptic axon, discouraging synaptic localization.
460 Conversely, it is possible that glycosylation is required for trafficking to the surface in the
461 first place, however this is less likely given that the levels of β-Dystroglycan were normal
462 in membrane-enriched lysate (**Fig. 1, Fig. 1 Supp. 2**).

463 A milder reduction in glycosylation (*B4gat1*$^{M155T/M155T}$) resulted in a cortical
464 migration phenotype that was restricted to midline (**Fig. 3 Supp. 4**) and a small
465 reduction in CCK^+/CB_1R^+ axon terminals and synaptic puncta density in CA1 which did
466 not appear to affect synapse function (**Figs. 3, 5-6**). The mildest reduction in
467 glycosylation amongst our models was observed in *Fkrp*$^{P448L/P448L}$ mutants, which
468 exhibited normal cortical migration but the same mild defect in CCK^+/CB_1R^+ IN axon
469 targeting and synaptic puncta density observed in *B4gat1*$^{M155T/M155T}$ mutants (**Figs. 3, 5-**
470 **6**). Together, these three glycosylation mutants illustrate the degree of
471 hypoglycosylation required for neurodevelopmental processes and show that defects in
472 synaptic function only arise in the context of severely reduced glycosylation; the residual
473 Dystroglycan function present in *B4gat1*$^{M155T/M155T}$ and *Fkrp*$^{P448L/P448L}$ mutants is
474 sufficient for most aspects of brain development. Finally, using *Dag1*$^{cyto/-}$ mutants that
475 lack the intracellular domain of Dystroglycan, we found that the intracellular domain
476 plays a role in some, but not all, neurodevelopmental processes. The intracellular
477 domain is not required for neuronal migration in neocortex or synapse formation in CA1
478 (**Figs. 2 and 5**) but is required for the proper targeting of CCK^+/CB_1R^+ IN axons in CA1-
479 3 (**Fig. 3**) and for subsequent CCK^+/CB_1R^+ IN basket synapse function (**Fig. 6**).
480

481 **Dystroglycan is an essential transsynaptic organizing molecule for CCK^+/CB_1R^+**
482 **basket synapses**

483 Synaptogenesis requires multiple distinct steps: (1) synaptic partner recognition,
484 (2) recruitment and assembly of core pre- and post-synaptic machinery, (3)
485 differentiation and maturation of synaptic identity, and (4) synaptic maintenance
486 (Südhof, 2018). Based on data from this study (**Fig. 4**) and previous work from our
487 group and others, mice lacking *Dystroglycan* exhibit defects in CCK^+/CB_1R^+ IN
488 development at the earliest time point they can be reliably identified (P0-P5), before the
489 peak phase of inhibitory synapse formation (P9), suggesting that Dystroglycan functions
490 at the earliest stages of synaptogenesis such as synaptic partner recognition (Favuzzi
491 et al., 2019). Determining the precise onset of synapse targeting and formation for most
492 IN subtypes, including CCK^+/CB_1R^+INs, is limited by a lack of genetic tools for
493 visualizing and manipulating IN subtypes during developmental stages.

494 The impairment in CCK^+/CB_1R^+ IN development throughout the forebrain
495 suggests a trans-synaptic role for Dystroglycan **(Fig. 3, Fig. 3 Supp. 4**). The identity of
496 the trans-synaptic binding partner between Dystroglycan-expressing cells and
497 CCK^+/CB_1R^+ INs remains unknown. Our data in *Emx1^{Cre};Pomt2^{cKO}* mice point to a
498 critical role for the glycan chains on Dystroglycan mediating this binding. All proteins
499 that bind to the glycan chains on Dystroglycan do so through at least one Laminin G
500 (LG) domain. There are over 25 LG-domain containing extracellular or transmembrane
501 proteins expressed in the hippocampus. Neurexins, a family of highly alternatively
502 spliced synaptic cell-adhesion molecules (*NRXN1-3*) which each contain multiple LG
503 domains, bind Dystroglycan in a glycosylation-dependent manner (Boucard et al., 2005;

504 Fuccillo et al., 2015; Reissner et al., 2014; Sugita et al., 2001). The specific splice
505 isoforms of *Nrxns* that bind Dystroglycan are expressed by CCK^+/CB_1R^+ INs (Fuccillo et
506 al., 2015; Ullrich et al., 1995). *Neurexin-3* conditional knockout (targeting all *Nrxn3*
507 isoforms) and CRISPR-mediated *Dag1* knockout both result in similar synaptic deficits
508 in olfactory bulb and prefrontal cortex (Trotter et al., 2023). While a Dystroglycan knock-
509 in mouse with reduced glycosylation that impairs Neurexin binding ($Dag1^{T190M}$) shows
510 normal CCK^+/CB_1R^+ synapse formation by immunohistochemistry, the functionality of
511 these synapses was not assessed by electrophysiology (Früh et al., 2016). Similar to
512 $B4gat1^{M155T/M155T}$ and $Fkrp^{P448L/P448L}$ mutants, the $Dag1^{T190M}$ mutation does not fully
513 eliminate Dystroglycan glycosylation, and therefore does not rule out the possibility that
514 Neurexins play a role at CCK^+/CB_1R^+ synapses. It is also possible that a yet
515 undescribed Dystroglycan interacting protein is required for initial synapse recognition,
516 and Nrxn-Dag1 interactions are required for subsequent synapse maturation and
517 maintenance only. Indeed, the majority of studies indicate that Neurexins are not
518 required for the initial formation of synapses, but rather regulate the maturation and
519 structural maintenance of synapses after they have formed (Chen et al., 2017;
520 Dudanova et al., 2007; Lin et al., 2023; Missler et al., 2003; Trotter et al., 2023).
521 Interestingly, while Dystroglycan localizes to both PV^+ and CCK^+/CB_1R^+ inhibitory
522 basket synapses in CA1, only the CCK^+/CB_1R^+ IN population was affected in the
523 dystroglycanopathy models (Früh et al., 2016). Presumably, PV^+ INs have a distinct
524 developmental program independent of Dystroglycan and likely require a different
525 postsynaptic recognition partner.
526

527 **A role for the Dystrophin-Glycoprotein Complex in CCK^+/CB_1R^+ interneuron**
528 **development**

529 In brain and muscle tissue, Dystroglycan forms a complex with Dystrophin and
530 several other proteins, collectively known as the Dystrophin Glycoprotein Complex
531 (DGC). Like Dystroglycan, Dystrophin is also expressed throughout the forebrain and is
532 associated with inhibitory synapses in multiple brain regions (Knuesel et al., 1999).
533 Patients with mutations in *Dystrophin* develop Duchenne Muscular Dystrophy (DMD),
534 and frequently exhibit cognitive impairments in the absence of brain malformations,
535 suggesting a general role for the DGC in synapse development and function (Jagadha
536 & Becker, 1988; Moizard et al., 2000; Naidoo & Anthony, 2020). A mouse model of
537 DMD lacking all neuronal Dystrophin isoforms (*mdx*) exhibits defects in CCK^+/CB_1R^+ IN
538 synapse development and abnormal innervation in the hippocampus, resembling the
539 innervation pattern we observed in $Emx1^{Cre};Dag1^{cKO}$ and $Emx1^{Cre};Pomt2^{cKO}$ mice in this
540 study (Krasowska et al., 2014). Since Dystroglycan interacts with Dystrophin through its
541 intracellular domain, we expected to observe similar phenotypes in mice lacking the
542 intracellular domain of Dystroglycan ($Dag1^{cyto/-}$). However, $Dag1^{cyto/-}$ showed a milder
543 axon targeting defect than $Emx1^{Cre};Dag1^{cKO}$ or *mdx* mice. In addition, IIH6 puncta were
544 normally localized to the somatodendritic compartment in $Dag1^{cyto/-}$ mutants, suggesting
545 that Dystroglycan does not require interactions with Dystrophin for is localization to
546 somatodendritic synapses. However, Dystroglycan's synaptic localization has not been
547 examined in the *mdx* mutants. Clearly, additional work is required to better understand
548 the relationship between Dystroglycan and Dystrophin at synapses in the brain.

549 While the density of CCK^+/CB_1R^+ IN synaptic puncta was normal in *Dag1*$^{cyto/-}$
550 mice, synaptic function was impaired to the same level as *Emx1*^{Cre}*;Dag*^{cKO} and
551 *Emx1*^{Cre}*;Pomt2*^{cKO} mice, and seizure latency was reduced. Given that *Dag1*$^{cyto/-}$ and
552 *B4gat1*$^{M155T/M155T}$ mutants show a similar reduction in Dystroglycan glycosylation (**Fig.**
553 **1B-C**), our observation that the functional synaptic phenotype is restricted to the
554 *Dag1*$^{cyto/-}$ mutant reinforces the notion that the intracellular domain of Dystroglycan
555 plays an active role in organizing essential postsynaptic signaling elements. One
556 possibility is that the intracellular domain of Dystroglycan is required to recruit additional
557 postsynaptic scaffolding elements and receptors necessary for CCK^+/CB_1R^+ basket
558 synapse function (Uezu et al., 2019). Importantly, *Dag1*$^{cyto/-}$ mice did not show a cortical
559 migration phenotype (**Fig. 2A-D**), indicating that the functional synaptic deficits and
560 reduced seizure latency occurred independent of cortical malformation.
561

562 **Altered inhibitory synapse development and function may contribute to**
563 **neurological symptoms in dystroglycanopathy**

564 In addition to muscular atrophy and hypotonia, dystroglycanopathy patients often
565 present with central nervous system symptoms. Patients with the most severe forms of
566 dystroglycanopathy (FCMD, Muscle-Eye-Brain disease, and Walker-Warburg
567 Syndrome) exhibit structural changes including hypoplasia of the retina, brainstem and
568 spinal cord, cerebellar cysts, hydrocephalus, Type II lissencephaly, and microcephaly,
569 associated with seizures and cognitive disability (Meilleur et al., 2014; Mercuri et al.,
570 2009). Patients with milder forms of dystroglycanopathy may show cognitive disability
571 and/or seizures without gross brain malformations, suggesting that there may be

572 synaptic deficits independent of early neurodevelopmental processes (e.g. neuronal
573 migration, axon guidance) (Mercuri et al., 2009; Yang et al., 2022). The mouse models
574 used in this study recapitulate the full spectrum of brain malformations seen in human
575 patients. *Emx1*^{Cre}*;Dag*^{cKO} and *Emx1*^{Cre}*;Pomt2*^{cKO} mice show Type II lissencephaly
576 consistent with severe dystroglycanopathy, whereas *B4gat1*$^{M155T/M155T}$ and
577 *Fkrp*$^{P448L/P448L}$ mutants have relatively normal cortical development consistent with mild
578 dystroglycanopathy. Mutations in any of the genes involved in the glycosylation of
579 Dystroglycan can result in dystroglycanopathy with seizures, but the incidence and
580 severity of seizures is higher in patients with brain malformations (Mercuri et al., 2009;
581 Wang et al., 2017; Yang et al., 2022).
582 Mice have been used to model dystroglycanopathy for decades, however to our
583 knowledge the present study is the first to investigate seizure susceptibility in mouse
584 models of dystroglycanopathy. It is probable that the CCK^+/CB_1R^+ interneuron axon
585 targeting and synapse phenotypes in the mouse models described in the present study
586 contribute to their seizure susceptibility and open the possibility that defective inhibitory
587 synaptic signaling mechanisms may underlie seizures in dystroglycanopathy patients.
588 Although severe neuronal migration phenotypes In *Emx1*^{Cre}*;Dag1*^{cKO} and
589 *Emx1*^{Cre}*;Pomt2*^{cKO} mice may contribute to seizure activity, our observation that *Dag1*$^{cyto/-}$
590 mutants showed both abnormal CCK^+/CB_1R^+synaptic function and reduced seizure
591 latency, with intact cortical migration, indicates that the seizure phenotype is likely
592 associated with synaptic defects. Supporting these results, CCK^+/CB_1R^+ interneurons in
593 the hippocampus are selectively lost in models of temporal lobe epilepsy with recurrent
594 seizures induced by pilocarpine. CCK^+/CB_1R^+ axons in CA1-3 begin to degenerate

595 within hours of status epilepticus, whereas PV^{+} INs are unaffected in this model
596 (Whitebirch et al., 2023; Wyeth et al., 2010).
597 While our *B4gat1*$^{M155T/M155T}$ mutants showed only a slightly reduced seizure
598 latency, the mutants experienced more severe seizures than the other mouse models,
599 resulting in death in 50% of cases (4/8 mutants compared to 0/6 fatalities among
600 littermate controls) (**Fig. 7 Supp. 1A**). Flurothyl-induced seizures are typically
601 generalized forebrain seizures; however in seizure-prone mouse models or in mice
602 exposed to higher concentrations of flurothyl, mice can experience a suppression of
603 brainstem oscillations followed by sudden death (Gu et al., 2022; Kadiyala et al., 2016).
604 The *B4gat1*$^{M155T/M155T}$ mutation was originally identified based on a hindbrain axon
605 guidance phenotype, suggesting they may have currently unknown defects in brainstem
606 development or circuitry that could render them more susceptible to fatal brainstem
607 seizures (Wright et al., 2012). Because the *Dag1* and *Pomt2* mutants are forebrain-
608 specific conditional knockouts, (**Fig. 1 Supp. 1A**), we would not anticipate abnormal
609 axon guidance in the brainstem or hindbrain of these mutants. Further research on the
610 nature and progression of seizures observed in mouse models may have a profound
611 impact on our understanding of dystroglycanopathy and potential therapeutic
612 interventions.
613
614 **Potential therapeutics for the restoration of synapse function in patients with**
615 **dystroglycanopathy**
616 Most patients with dystroglycanopathy present with mutations in one of the 19
617 genes required for the glycosylation of Dystroglycan, resulting in hypoglycosylated

618 Dystroglycan. We have demonstrated that a mild reduction in the glycosylation of
619 Dystroglycan, as seen in *Fkrp*$^{P448L/P448L}$ and *B4gat1*$^{M155T/M155T}$ mutants, does not
620 significantly disrupt synapse function. This suggests that glycosylation may not need to
621 be restored to wild-type levels in order to achieve normal synapse function. Gene
622 replacement therapy may be well suited to treat certain forms of dystroglycanopathy by
623 rescuing glycosylation. AAV-mediated delivery of fully functional glycosyltransferases
624 has been shown to significantly improve muscle pathology and function in dystrophic
625 mice, however synaptic phenotypes have not been examined (Kanagawa, 2021).
626 Supplementation with (CDP)-ribitol, which is synthesized by *CRPPA* (previously known
627 as *ISPD*), can restore functional Dystroglycan glycosylation and improve muscle
628 function in mouse models with hypomorphic mutations in *CRPPA* or *Fkrp* (Cataldi et al.,
629 2018). In mice lacking functional *CRPPA* or *Fkrp* in skeletal muscle, (CDP)-ribitol can
630 further enhance the therapeutic impact of gene restoration (Cataldi et al., 2020).
631 However, whether (CDP)-ribitol treatment can improve Dystroglycan function in other
632 models of dystroglycanopathy, or is capable of restoring Dystroglycan glycosylation and
633 synaptic function in the nervous system, remains untested.
634

635 **CONCLUSION**

636 We demonstrate that Dystroglycan is critical for the postnatal development of
637 CCK^+/CB_1R^+ interneuron axon targeting and synapse formation/function in the
638 hippocampus of severe mouse models of dystroglycanopathy. Extracellular
639 glycosylation of Dystroglycan and intracellular interactions involving the cytoplasmic
640 domain are both essential for Dystroglycan's synaptic organizing role. Mice with a

641 partial reduction in glycosylation have relatively normal CCK^+/CB_1R^+ interneuron axon
642 targeting and synapse function, suggesting that even a partial restoration of
643 glycosylation may have some therapeutic benefit. These findings suggest that
644 CCK^+/CB_1R^+ interneuron axon targeting defects may contribute to cognitive
645 impairments and seizure susceptibility in dystroglycanopathy.
646

647 **MATERIALS AND METHODS**

648 **Animal husbandry**

649 All animals were housed and cared for by the Department of Comparative
650 Medicine (DCM) at Oregon Health and Science University (OHSU), an AAALAC-
651 accredited institution. Animal procedures were approved by OHSU Institutional Animal
652 Care and Use Committee (Protocol # IS00000539), adhered to the NIH *Guide for the*
653 *care and use of laboratory animals*, and provided with 24-hour veterinary care. Animal
654 facilities are regulated for temperature and humidity and maintained on a 12-hour light-
655 dark cycle and were provided food and water *ad libitum*. Animals older than postnatal
656 day 6 (P6) were euthanized by administration of CO_2, animals <P6 were euthanized by
657 rapid decapitation.
658

659 **Mouse strains and genotyping**

660 The day of birth was designated postnatal day 0 (P0). Ages of mice used for
661 each analysis are indicated in the figure and figure legends. Mouse strains used in this
662 study have been previously described and were obtained from Jackson Labs, unless
663 otherwise indicated (**Table 1**) (Chan et al., 2010; Cohn et al., 2002; Goebbels et al.,

664 2006; Gorski et al., 2002; Hu et al., 2011; Peron et al., 2015; Satz et al., 2009; Tronche
665 et al., 1999; Wright et al., 2012). Breeding schemas are as described in **Table 2**. Where
666 possible, mice were maintained on a C57BL/6 background. *Dag1*$^{cyto/-}$ mice occurred at a
667 frequency lower than Mendelian, suggesting that a proportion of progeny die
668 embryonically. To increase viability of pups, the *Dag1*^{cyto} line was outcrossed to a CD-1
669 background for one generation. The *B4gat1* line has a mixed genetic background: it was
670 founded on a C3H/He background and then crossed on to C57BL/6 for future
671 generations. Genomic DNA extracted from toe or tail samples (Quanta BioSciences)
672 was used to genotype animals. Primers for genotyping can be found on the JAX
673 webpage or originating article. For each mouse strain, littermate controls were used for
674 comparison with mutant mice. For all experiments, unless otherwise noted, mice of both
675 sexes were used indiscriminately. See **Supplementary Table 1** for a summary of sexes
676 used in each experiment.
677

678 **Table 1. Mouse strains**

Common name	Strain name	Reference	Stock #
Dag1^{Flox}	*B6.129(Cg)-Dag1*$^{tm2.1Kcam}$*/J*	(Cohn et al., 2002)	009652
Dag1^{cyto}	N/A	(Satz et al., 2009)	N/A
Pomt2^{Flox}	*POMT2tm1.1Hhu/J*	(Hu et al., 2011)	017880
B4gat1^{M155T}	*B6(C3)-B4GAT1*^{m1Ddg}*/J*	(Wright et al., 2012)	022018
Fkrp^{P448L}	*C57BL/6NJ-Fkrp*^{em1Lgmd}*/J*	(Chan et al., 2010)	034659
R26$^{LSL-H2B-mCherry}$	*B6.Gt(ROSA)26Sor*$^{tm1.1Ksvo}$	(Peron et al., 2015)	023139
Emx1^{Cre}	*B6.129S2-Emx1*$^{tm1(cre)Krj}$*/J*	(Gorski et al., 2002)	005628
Nestin^{Cre}	*B6.Cg-Tg(Nes-cre)*^{1Kln}*/J*	(Tronche et al., 1999)	003771
NEX^{Cre}	*NeuroD6*$^{tm1(cre)Kan}$	(Goebbels et al., 2006)	MGI:4429523

679

680 **Table 2. Breeding schemes**

Breeding Scheme	Control Genotype	Mutant Genotype

Emx1$^{Cre/+}$;Dag1$^{+/-}$ x Dag1$^{Flox/Flox}$	*Emx1$^{Cre/+}$;Dag1$^{Flox/+}$*	*Emx1$^{Cre/+}$;Dag1$^{Flox/-}$*
Nestin$^{Cre/+}$;Dag1$^{+/-}$ x Dag1$^{Flox/Flox}$	*Nestin$^{Cre/+}$;Dag1$^{Flox/+}$*	*Nestin$^{Cre/+}$;Dag1$^{Flox/-}$*
NEX$^{Cre/+}$;Dag1$^{+/-}$ x Dag1$^{Flox/Flox}$	*NEX$^{Cre/+}$;Dag1$^{Flox/+}$*	*NEX$^{Cre/+}$;Dag1$^{Flox/-}$*
Emx1$^{Cre/+}$;Pomt2$^{Flox/+}$ x Pomt2$^{Flox/Flox}$	*Emx1$^{Cre/+}$;Pomt2$^{Flox/+}$*	*Emx1$^{Cre/+}$;Pomt2$^{Flox/Flox}$*
Dag1$^{cyto/+}$ x Dag1$^{+/-}$	*WT*	*Dag1$^{cyto/-}$*
B4gat1$^{M155T/+}$ x B4gat1$^{M155T/+}$	*WT*	*B4gat1$^{M155T/M155T}$*
Fkrp$^{P448L/+}$ x Fkrp$^{P448L/+}$	*WT*	*Fkrp$^{P448L/P448L}$*

Perfusions and tissue preparation

Brains from mice younger than P15 were dissected and drop fixed in 5 mLs of 4% paraformaldehyde (PFA) in phosphate buffered saline (PBS) overnight for 18-24 hours at 4°C. Mice P15 and older were deeply anesthetized using CO2 and transcardially perfused with ice cold 0.1M PBS for two minutes to clear blood from the brain, followed by 15 mLs of ice cold 4% PFA in PBS. After perfusion, brains were dissected and post-fixed in 4% PFA for 30 minutes at room temperature. Brains were rinsed with PBS, embedded in 4% low-melt agarose (Fisher cat. no. 16520100), and sectioned at 50µm using a vibratome (VT1200S, Leica Microsystems Inc., Buffalo Grove, IL) into 24-well plates containing 1 mL of 0.1M PBS with Sodium Azide.

Immunohistochemistry

Single and multiple immunofluorescence detection of antigens was performed as follows: free-floating vibratome sections (50µm) were briefly rinsed with PBS, then blocked for 1 hour in PBS containing 0.2% Triton-X (PBST) plus 10% normal goat or donkey serum. Sections were incubated with primary antibodies (**Table 3**) diluted in blocking solution at 4°C for 48-72 hours. For staining of Dystroglycan synaptic puncta, an antigen retrieval step was performed prior to incubation in primary antibody. Briefly,

700 sections were incubated in sodium citrate solution for 15 min at 95 degrees in a water
701 bath. Following incubation in primary antibody, sections were rinsed with PBS then
702 washed with PBST three times for 20 min each. Sections were then incubated with a
703 cocktail of secondary antibodies (1:500, Alexa Fluor 488, 546, 647) in blocking solution
704 overnight at room temperature. Sections were washed with PBS three times for 20 min
705 each and counterstained with Hoechst 33342 (1:10,000, Life Technologies, Cat#
706 H3570) for 20 min to visualize nuclei. Finally, sections were mounted on slides using
707 Fluoromount-G (SouthernBiotech) and sealed using nail polish.
708

709 **Table 3. Primary antibodies used for immunohistochemistry**

Target	Host	Dilution	Source	Catalog #	RRID
α-Dystroglycan (IIH6C4)	Mouse	1:250	Millipore	05-593	AB_309828
β-Dystroglycan	Mouse	1:50	Leica Biosystems	NCL-b-DG	AB_442043
CB1R	Guinea pig	1:1000	Synaptic Systems	258-104	AB_2661870
Cux1	Rabbit	1:500	Santa Cruz Biotech	sc-13024	AB_2261231
Laminin	Rabbit	1:1000	Sigma	L9393	AB_477163
NECAB1	Rabbit	1:500	Sigma	HPA023629	AB1848014
NECAB2	Rabbit	1:500	Proteintech	12257-1-AP	AB_2877841
NeuN	Mouse	1:250	Millipore	MAB377	AB_2298772
Parvalbumin	Rabbit	1:1000	Swant	PV27	AB_2631173
Parvalbumin	Mouse	1:50	Swant	235	AB_10000343
Somatostatin	Rabbit	1:2000	Peninsula Labs	T-4103	AB_518614
Tbr1	Rabbit	1:500	Millipore	AB10554	AB_10806888
VGAT	Rabbit	1:500	Synaptic Systems	131-003	AB_887869
VGAT	Guinea Pig	1:500	Synaptic Systems	131-005	AB_1106810
VGlut3	Rabbit	1:1000	Synaptic Systems	135-203	AB_887886
VIP	Rabbit	1:1000	ImmunoStar	20077	AB_572270

710

711 **Microscopy**

712 Imaging was performed on either a Zeiss Axio Imager M2 fluorescence upright
713 microscope equipped with an Apotome.2 module or a Zeiss LSM 980 laser scanning
714 confocal build around a motorized Zeiss Axio Observer Z1 inverted microscope with a
715 Piezo stage. The Axio Imager M2 uses a metal halide light source (HXP 200 C),
716 Axiocam 506 mono camera, and 10X/0.3 NA EC Plan-Neofluar, 20X/0.8 NA Plan-
717 Apochromat objectives. The LSM 980 confocal light path has two multi-alkali PMTs and
718 two GaAsP PMTs for four track imaging. Confocal images were acquired using a
719 63X/1.4 NA Plan-Apochromat Oil DIC M27 objective. Z-stack images were acquired and
720 analyzed offline in ImageJ/FIJI (Schindelin et al., 2012) or Imaris 9.8 (Oxford
721 Instruments). Images used for quantification between genotypes were acquired using
722 the same exposure times. Brightness and contrast were adjusted in FIJI to improve
723 visibility of images for publication. Figures were composed in Adobe Illustrator 2023
724 (Adobe Systems).

725

726 **Image Quantification**

727 For imaging experiments, 4-8 images were acquired from 2-4 coronal sections per
728 animal, and at least three animals per genotype were used for analysis.

729 *Cortical Lamination*

730 Images of somatosensory cortex were acquired using a 10X objective on a Zeiss Axio
731 Imager M2. 4μm z-stacks covering 16μm were acquired and multiple tiles were stitched
732 together. Maximum projections were used for analysis. In FIJI, the straight line tool with
733 a 300μm line width was used to measure the fluorescence profile from corpus callosum

734 to pial surface. Background fluorescence was determined as the average fluorescence
735 of the 20 darkest pixels; background was then subtracted from all points. The cortical
736 distance was broken into 10 bins and average fluorescence within each bin was
737 compared between genotypes.

738 *Hippocampal CA1 CB_1R and PV Distribution*

739 Images of dorsal hippocampal CA1 were acquired using a 20X objective on a Zeiss
740 Axio Imager M2. Maximum projection images of 0.6μm z-stacks covering 9μm were
741 analyzed in FIJI. The straight line tool with a 300μm line width was used to measure the
742 fluorescence profile within SO, SP, and SR of CA1, avoiding Parvalbumin$^+$ cell bodies.
743 Background fluorescence was determined as the average fluorescence of the 50
744 darkest pixels; background was then subtracted from all points. The thickness of SP
745 was determined using Hoechst fluorescence. Average fluorescence within SO/SP/SR
746 was compared between genotypes.

747 *Interneuron Cell Counts in CA1*

748 Images of dorsal hippocampal CA1 were acquired using a 10X objective on a Zeiss
749 Axio Imager M2. Maximum projection images of 4μm z-stacks covering 40μm were
750 analyzed in FIJI. Immunolabeled NECAB1/NECAB2/PV cell bodies were counted if they
751 were within 100μm of *stratum pyramidale*. The freehand line tool was used to measure
752 the length of *stratum pyramidale*. Cell number was normalized to the length of *stratum*
753 *pyramidale* present in the analyzed region.

754 *Hippocampal CB_1R/PV/VGAT Density and Co-localization*

755 Images of dorsal hippocampal CA1 were acquired using a 63X objective on a Zeiss
756 LSM 980. 0.2μm z-stacks covering 3μm were analyzed in Imaris. Hoechst fluorescence

757 was used to determine the bounds of SP. The Imaris Spots function was used to
758 determine the location of synaptic puncta in 3-dimensional space. Synaptic puncta were
759 deemed to be co-localized if they were within 1μm of each other.
760
761 **Western Blot**
762 Cortex or hippocampus was dissected and solubilized in 1 mL of lysis buffer containing
763 100mM NaCl, 50nM Tris, 2.5mM $CaCl_2$, 1% Triton X-100, 1% n-Octyl-β-D-
764 glucopyranoside, and protease inhibitors. Lysate was incubated at 4°C for 1 hour and
765 then spun at 12,500g for 25 minutes. Supernatant containing 3,000μg (cortex) or
766 2,000μg (hippocampus) of protein (as determined by Pierce BCA Protein Assay) was
767 applied to agarose-bound Wheat Germ Agglutinin (WGA) (Vector Labs) overnight at
768 4°C. Beads were washed 3X in TBS and boiled in 1X LDS sample buffer with 2-
769 Mercaptoethanol (1:100) for 5 minutes. Samples were run on a 4-15% gradient
770 polyacrylamide gel at 100V for 75 minutes and then transferred to a PVDF membrane
771 (100V for 100 minutes). For immunoblotting, membranes were blocked in 5% milk TBST
772 and then incubated overnight at 4°C in 5% milk TBST containing primary antibody.
773 Antibodies used: α-Dystroglycan (IIH6C4) (Millipore cat. no. 05-593, mouse IgM, 1:500),
774 MANDAG2 (DSHB cat. no. 7D11, mouse IgG1, 1:500), β3-tubulin (Cell Signaling
775 Technology cat. no. 5568, rabbit, 1:2000). Membranes were washed 3X in TBST and
776 incubated on fluorescent IRDye secondary antibody (1:10,000, LI-COR) in 5% milk
777 TBST for 1 hour at room temperature. Membranes were imaged using a LI-COR
778 Odyssey CLx 0918 imager and signal analyzed using LI-COR Image Studio Lite version
779 5.2.

780

781 **Electrophysiology**

782 For acute slice preparation, mice were deeply anesthetized in 4% isoflurane and
783 subsequently injected with a lethal dose of 2% 2, 2, 2-Tribromoethanol in sterile water
784 followed by transcardial perfusion with 10 mL ice cold cutting solution containing the
785 following (in mM): 93 NMDG, 2.5 KCl, 1.2 NaH_2PO_4, 30 $NaHCO_3$, 20 HEPES, 24
786 glucose, 5 Na Ascorbate, 2 Thiourea, 3 Na Pyruvate, 13 N-Acetyl Cysteine, 1 Kynurenic
787 acid, 10 $MgSO_4$, 0.5 $CaCl_2$; pH 7.3, 300-340mmol/kg. After rapid decapitation, the brain
788 was briefly submerged in ice cold cut solution bubbled with carbogen (95% oxygen, 5%
789 CO2) and then sectioned into 300µm sagittal sections (Leica VT1200S vibratome) in
790 bubbled ice-cold cut solution. Slices were recovered in 37°C cut solution, bubbled, for
791 15 minutes followed by 1 hour in room temperature recording ACSF (containing, in mM:
792 125 NaCl, 25 $NaHCO_3$, 1.25 NaH_2PO_4, 3 KCl, 25 D-Glucose, 2 $CaCl_2$, 1 $MgCl_2$) with an
793 osmolarity of 310-320mmol/kg and supplemented with 1.5mM Na Ascorbate, bubbled.

794 CA1 pyramidal cells were patched in whole cell configuration using 3-5MΩ
795 borosilicate glass pipettes filled with high chloride internal solution containing the
796 following (in mM): 125 CsCl, 2.5 $MgCl_2$, 0.5 EGTA, 10 HEPES, 2 Mg-ATP, 0.3 Na-GTP,
797 5 QX-314; pH 7.2, 300mmol/kg. Pipettes were wrapped in parafilm to reduce capacitive
798 currents. Cells were voltage clamped at -70mV and continuously superfused with 2-3
799 mL/min bubbled recording ACSF (310-320mmol/kg) containing 10µM NBQX to block
800 excitatory transmission. Recordings were performed at 34°C. After 5 minutes of
801 spontaneous IPSC (sIPSC) recording, 10µM Carbachol was added to the perfusate and
802 another 5 minutes of sIPSC were recorded. Slices were discarded after exposure to

803 Carbachol. Signals were amplified with an AxoPatch 200B amplifier (Molecular
804 Devices), low-pass filtered at 5 kHz, and digitized and sampled at 10 kHz with a NIDAQ
805 analog-to-digital board (National Instruments). Data were acquired and analyzed using
806 a custom script in Igor Pro 8 (Wavemetrics). A hyperpolarizing step of -10mV was
807 applied before each sweep to monitor input resistance, series resistance, and measure
808 cell capacitance. Series resistance was not compensated and was maintained below
809 20MΩ. Cells were excluded if series resistance changed by more than 25%.
810 To calculate the proportion of cells that responded to Carbachol, cells were
811 sorted into “responsive” and “non-responsive” categories. Cells were categorized as
812 responsive if sIPSC frequency increased by 20% or more with the addition of
813 Carbachol. If sIPSC frequency in a cell changed by less than 20% or less than 0.5Hz it
814 was deemed non-responsive.
815
816 **Flurothyl Seizure Induction**
817 Mice aged P40-P55 were used for the flurothyl-induced seizure susceptibility assay to
818 determine seizure threshold. Briefly, mice were placed in an enclosed glass chamber
819 equipped with a vaporization chamber out of reach of the mouse. Volatile liquid 10% Bis
820 (2,2,2-Trifluorotheyl) Ether (Millipore Sigma cat. no 287571) in 95% EtOH was delivered
821 to the vaporization chamber at a rate of 6 mL/hour. Seizure latency was determined as
822 the amount of time until generalized tonic-clonic seizure (TCS). Upon exhibiting TCS,
823 animals were immediately removed from the chamber and returned to their home cage,
824 whereupon seizures ceased rapidly. Sample size was determined using power analysis
825 as described below. The *Emx1*^{Cre}*;Dag1* experimental groups were powered sufficiently

826 to determine sex differences. Because no sex difference was found (**Fig. 7 Supp. 1C**),
827 sexes were pooled for the remaining experiments. For statistical tests, outliers were
828 excluded. Outliers were calculated as follows: first, the interquartile range (IQR) was
829 calculated and multiplied by 1.5. This 1.5*IQR value was subtracted from the 25%
830 quartile (Q1) and added to the 75% quartile (Q3). Points outside of the range Q1 -
831 1.5*IQR < x < Q3 + 1.5*IQR were categorized as outliers and indicated as such on all
832 graphs. This was done to remove bias from extreme outliers observed in this
833 experiment.
834
835 **Statistical analysis**
836 Phenotypic analyses were conducted using tissue collected from at least three
837 mice per genotype from at least two independent litters. The number of mice and
838 replicates used for each analysis ("N") are indicated in **Supplementary Table 1**. Power
839 analysis using pilot data was used to determine samples sizes with $\alpha = 0.05$ and $\beta =$
840 0.80. Phenotypes were indistinguishable between male and female mice and were
841 analyzed together. In many cases, highly penetrant phenotypes revealed the genotypes
842 of the mice and no blinding could be performed. For comparisons between two groups,
843 significance was determined using a two-tailed Students t-test. For comparisons
844 between more than two groups, significance was determined using a 2-way ANOVA
845 with Tukey HSD post-hoc analysis. Statistical significance was set at $\alpha = 0.05$ ($p < 0.05$)
846 and data presented as means ± SEM. Statistical analyses and data visualization were
847 performed in R (version 4.0.2).
848

DATA AVAILABILITY

The data that support the findings of this study are available from the corresponding author upon reasonable request.

REFERENCES

Barresi, R., & Campbell, K. P. (2006). Dystroglycan: From biosynthesis to pathogenesis of human disease. *Journal of Cell Science*, *119*(2), 199–207. https://doi.org/10.1242/jcs.02814

Beedle, A. M., Turner, A. J., Saito, Y., Lueck, J. D., Foltz, S. J., Fortunato, M. J., Nienaber, P. M., & Campbell, K. P. (2012). Mouse fukutin deletion impairs dystroglycan processing and recapitulates muscular dystrophy. *The Journal of Clinical Investigation*, *122*(9), 3330–3342. https://doi.org/10.1172/JCI63004

Berghuis, P., Rajnicek, A. M., Morozov, Y. M., Ross, R. A., Mulder, J., Urbán, G. M., Monory, K., Marsicano, G., Matteoli, M., Canty, A., Irving, A. J., Katona, I., Yanagawa, Y., Rakic, P., Lutz, B., Mackie, K., & Harkany, T. (2007). Hardwiring the brain: Endocannabinoids shape neuronal connectivity. *Science (New York, N.Y.)*, *316*(5828), 1212–1216. https://doi.org/10.1126/science.1137406

Blaeser, A., Keramaris, E., Chan, Y. M., Sparks, S., Cowley, D., Xiao, X., & Lu, Q. L. (2013). Mouse models of fukutin-related protein mutations show a wide range of disease phenotypes. *Human Genetics*, *132*(8), 923–934. https://doi.org/10.1007/s00439-013-1302-7

Boucard, A. A., Chubykin, A. A., Comoletti, D., Taylor, P., & Südhof, T. C. (2005). A Splice Code for trans-Synaptic Cell Adhesion Mediated by Binding of Neuroligin 1 to α- and β-Neurexins. *Neuron*, *48*(2), 229–236. https://doi.org/10.1016/j.neuron.2005.08.026

Briatore, F., Patrizi, A., Viltono, L., Sassoe-Pognetto, M., & Wulff, P. (2010). Quantitative organization of GABAergic synapses in the molecular layer of the

mouse cerebellar cortex. *PLoS ONE*, *5*(8). https://doi.org/10.1371/journal.pone.0012119

Briatore, F., Pregno, G., Di Angelantonio, S., Frola, E., De Stefano, M. E., Vaillend, C., Sassoè-Pognetto, M., & Patrizi, A. (2020). Dystroglycan Mediates Clustering of Essential GABAergic Components in Cerebellar Purkinje Cells. *Frontiers in Molecular Neuroscience*, *13*, 164. https://doi.org/10.3389/fnmol.2020.00164

Brockington, M., Blake, D. J., Prandini, P., Brown, S. C., Torelli, S., Benson, M. A., Ponting, C. P., Estournet, B., Romero, N. B., Mercuri, E., Voit, T., Sewry, C. A., Guicheney, P., & Muntoni, F. (2001). Mutations in the Fukutin-Related Protein Gene (FKRP) Cause a Form of Congenital Muscular Dystrophy with Secondary Laminin α2 Deficiency and Abnormal Glycosylation of α-Dystroglycan. *The American Journal of Human Genetics*, *69*(6), 1198–1209. https://doi.org/10.1086/324412

Brünig, I., Suter, A., Knuesel, I., Lüscher, B., & Fritschy, J. M. (2002). GABAergic Terminals Are Required for Postsynaptic Clustering of Dystrophin but Not of GABAA Receptors and Gephyrin. *Journal of Neuroscience*, *22*(12), 4805–4813. https://doi.org/10.1523/jneurosci.22-12-04805.2002

Cataldi, M. P., Blaeser, A., Lu, P., Leroy, V., & Lu, Q. L. (2020). ISPD Overexpression Enhances Ribitol-Induced Glycosylation of α-Dystroglycan in Dystrophic FKRP Mutant Mice. *Molecular Therapy - Methods & Clinical Development*, *17*, 271–280. https://doi.org/10.1016/j.omtm.2019.12.005

Cataldi, M. P., Lu, P., Blaeser, A., & Lu, Q. L. (2018). Ribitol restores functionally glycosylated α-dystroglycan and improves muscle function in dystrophic FKRP-

mutant mice. *Nature Communications*, *9*(1), Article 1. https://doi.org/10.1038/s41467-018-05990-z

Chan, Y. M., Keramaris-Vrantsis, E., Lidov, H. G., Norton, J. H., Zinchenko, N., Gruber, H. E., Thresher, R., Blake, D. J., Ashar, J., Rosenfeld, J., & Lu, Q. L. (2010). Fukutin-related protein is essential for mouse muscle, brain and eye development and mutation recapitulates the wide clinical spectrums of dystroglycanopathies. *Human Molecular Genetics*, *19*(20), 3995–4006. https://doi.org/10.1093/hmg/ddq314

Chen, L. Y., Jiang, M., Zhang, B., Gokce, O., & Südhof, T. C. (2017). Conditional Deletion of All Neurexins Defines Diversity of Essential Synaptic Organizer Functions for Neurexins. *Neuron*, *94*(3), 611-625.e4. https://doi.org/10.1016/j.neuron.2017.04.011

Clement, E., Mercuri, E., Godfrey, C., Smith, J., Robb, S., Kinali, M., Straub, V., Bushby, K., Manzur, A., Talim, B., Cowan, F., Quinlivan, R., Klein, A., Longman, C., McWilliam, R., Topaloglu, H., Mein, R., Abbs, S., North, K., … Muntoni, F. (2008). Brain involvement in muscular dystrophies with defective dystroglycan glycosylation. *Annals of Neurology*, *64*(5), 573–582. https://doi.org/10.1002/ana.21482

Cohn, R. D., Henry, M. D., Michele, D. E., Barresi, R., Saito, F., Moore, S. A., Flanagan, J. D., Skwarchuk, M. W., Robbins, M. E., Mendell, J. R., Williamson, R. A., & Campbell, K. P. (2002). Disruption of Dag1 in differentiated skeletal muscle reveals a role for dystroglycan in muscle regeneration. *Cell*, *110*(5), 639–648. https://doi.org/10.1016/S0092-8674(02)00907-8

Colognato, H., Galvin, J., Wang, Z., Relucio, J., Nguyen, T., Harrison, D., Yurchenco, P. D., & Ffrench-Constant, C. (2007). Identification of dystroglycan as a second laminin receptor in oligodendrocytes, with a role in myelination. *Development*, *134*(9), 1723–1736. https://doi.org/10.1242/dev.02819

Dhaibani, M. A. A., El-Hattab, A. W., Ismayl, O., & Suleiman, J. (2018). B3GALNT2-Related Dystroglycanopathy: Expansion of the Phenotype with Novel Mutation Associated with Muscle-Eye-Brain Disease, Walker–Warburg Syndrome, Epileptic Encephalopathy-West Syndrome, and Sensorineural Hearing Loss. *Neuropediatrics*, *49*(4), 289–295. https://doi.org/10.1055/s-0038-1651519

Di Rosa, G., Messina, S., D'Amico, A., Bertini, E., Pustorino, G., Spanò, M., & Tortorella, G. (2011). A new form of alpha-dystroglycanopathy associated with severe drug-resistant epilepsy and unusual EEG features. *Epileptic Disorders*, *13*(3), 259–262. https://doi.org/10.1684/epd.2011.0461

Dudanova, I., Tabuchi, K., Rohlmann, A., Südhof, T. C., & Missler, M. (2007). Deletion of α-neurexins does not cause a major impairment of axonal pathfinding or synapse formation. *Journal of Comparative Neurology*, *502*(2), 261–274. https://doi.org/10.1002/cne.21305

Durbeej, M., Henry, M. D., Ferletta, M., Campbell, K. P., & Ekblom, P. (1998). Distribution of dystroglycan in normal adult mouse tissues. *Journal of Histochemistry and Cytochemistry*, *46*(4), 449–457. https://doi.org/10.1177/002215549804600404

Egawa, K., Nakakubo, S., Kimura, S., Goto, T., Manabe, A., & Shiraishi, H. (2021). Flurothyl-induced seizure paradigm revealed higher seizure susceptibility in

middle-aged Angelman syndrome mouse model. *Brain and Development*, *43*(4), 515–520. https://doi.org/10.1016/j.braindev.2020.12.011

Eggan, S. M., Mizoguchi, Y., Stoyak, S. R., & Lewis, D. A. (2010). Development of Cannabinoid 1 Receptor Protein and Messenger RNA in Monkey Dorsolateral Prefrontal Cortex. *Cerebral Cortex*, *20*(5), 1164–1174. https://doi.org/10.1093/cercor/bhp179

Ervasti, J. M., & Campbell, K. P. (1991). Membrane organization of the dystrophin-glycoprotein complex. *Cell*, *66*(6), 1121–1131. https://doi.org/10.1016/0092-8674(91)90035-W

Favuzzi, E., Deogracias, R., Marques-Smith, A., Maeso, P., Jezequel, J., Exposito-Alonso, D., Balia, M., Kroon, T., Hinojosa, A. J., F. Maraver, E., & Rico, B. (2019). Distinct molecular programs regulate synapse specificity in cortical inhibitory circuits. *Science*, *363*(6425), 413–417. https://doi.org/10.1126/science.aau8977

Földy, C., Neu, A., Jones, M. V., & Soltesz, I. (2006). Presynaptic, activity-dependent modulation of cannabinoid type 1 receptor-mediated inhibition of GABA release. *The Journal of Neuroscience: The Official Journal of the Society for Neuroscience*, *26*(5), 1465–1469. https://doi.org/10.1523/JNEUROSCI.4587-05.2006

Freund, T. F., & Katona, I. (2007). Perisomatic inhibition. *Neuron*, *56*(1), 33–42. https://doi.org/10.1016/j.neuron.2007.09.012

Früh, S., Romanos, J., Panzanelli, P., Bürgisser, D., Tyagarajan, S. K., Campbell, K. P., Santello, M., & Fritschy, J. M. (2016). Neuronal dystroglycan is necessary for

formation and maintenance of functional CCK-positive basket cell terminals on pyramidal cells. *Journal of Neuroscience*, *36*(40), 10296–10313. https://doi.org/10.1523/JNEUROSCI.1823-16.2016

Fuccillo, M. V., Földy, C., Gökce, Ö., Rothwell, P. E., Sun, G. L., Malenka, R. C., & Südhof, T. C. (2015). Single-Cell mRNA Profiling Reveals Cell-Type-Specific Expression of Neurexin Isoforms. *Neuron*, *87*(2), 326–340. https://doi.org/10.1016/j.neuron.2015.06.028

Gerin, I., Ury, B., Breloy, I., Bouchet-Seraphin, C., Bolsée, J., Halbout, M., Graff, J., Vertommen, D., Muccioli, G. G., Seta, N., Cuisset, J.-M., Dabaj, I., Quijano-Roy, S., Grahn, A., Van Schaftingen, E., & Bommer, G. T. (2016). ISPD produces CDP-ribitol used by FKTN and FKRP to transfer ribitol phosphate onto α-dystroglycan. *Nature Communications*, *7*(1), Article 1. https://doi.org/10.1038/ncomms11534

Godfrey, C., Clement, E., Mein, R., Brockington, M., Smith, J., Talim, B., Straub, V., Robb, S., Quinlivan, R., Feng, L., Jimenez-Mallebrera, C., Mercuri, E., Manzur, A. Y., Kinali, M., Torelli, S., Brown, S. C., Sewry, C. A., Bushby, K., Topaloglu, H., … Muntoni, F. (2007). Refining genotype–phenotype correlations in muscular dystrophies with defective glycosylation of dystroglycan. *Brain*, *130*(10), 2725–2735. https://doi.org/10.1093/brain/awm212

Goebbels, S., Bormuth, I., Bode, U., Hermanson, O., Schwab, M. H., & Nave, K.-A. (2006). Genetic targeting of principal neurons in neocortex and hippocampus of NEX-Cre mice. *Genesis*, *44*(12), 611–621. https://doi.org/10.1002/dvg.20256

Gorski, J. A., Talley, T., Qiu, M., Puelles, L., Rubenstein, J. L. R., & Jones, K. R. (2002). Cortical Excitatory Neurons and Glia, But Not GABAergic Neurons, Are Produced in the Emx1-Expressing Lineage. *Journal of Neuroscience*, *22*(15), 6309–6314. https://doi.org/10.1523/JNEUROSCI.22-15-06309.2002

Gu, B., Levine, N. G., Xu, W., Lynch, R. M., Pardo-Manuel de Villena, F., & Philpot, B. D. (2022). Ictal neural oscillatory alterations precede sudden unexpected death in epilepsy. *Brain Communications*, *4*(2), fcac073. https://doi.org/10.1093/braincomms/fcac073

Holt, K. H., Crosbie, R. H., Venzke, D. P., & Campbell, K. P. (2000). Biosynthesis of dystroglycan: Processing of a precursor propeptide. *FEBS Letters*, *468*(1), 79–83. https://doi.org/10.1016/S0014-5793(00)01195-9

Holzfeind, P. J., Grewal, P. K., Reitsamer, H. A., Kechvar, J., Lassmann, H., Hoeger, H., Hewitt, J. E., & Bittner, R. E. (2002). Skeletal, cardiac and tongue muscle pathology, defective retinal transmission, and neuronal migration defects in the Largemyd mouse defines a natural model for glycosylation-deficient muscle – eye – brain disorders. *Human Molecular Genetics*, *11*(21), 2673–2687. https://doi.org/10.1093/hmg/11.21.2673

Hu, H., Li, J., Gagen, C. S., Gray, N. W., Zhang, Z., Qi, Y., & Zhang, P. (2011). Conditional knockout of protein O-mannosyltransferase 2 reveals tissue-specific roles of O-mannosyl glycosylation in brain development. *Journal of Comparative Neurology*, *519*(7), 1320–1337. https://doi.org/10.1002/cne.22572

Hu, H., Liu, Y., Bampoe, K., He, Y., & Yu, M. (2016). Postnatal Gene Therapy Improves Spatial Learning Despite the Presence of Neuronal Ectopia in a Model of

Neuronal Migration Disorder. *Genes*, *7*(12), Article 12. https://doi.org/10.3390/genes7120105

Ibraghimov-Beskrovnaya, O., Ervasti, J. M., Leveille, C. J., Slaughter, C. A., Sernett, S. W., & Campbell, K. P. (1992). Primary structure of dystrophin-associated glycoproteins linking dystrophin to the extracellular matrix. *Nature*, *355*(6362), 696–702. https://doi.org/10.1038/355696a0

Jagadha, V., & Becker, L. E. (1988). Brain morphology in Duchenne muscular dystrophy: A Golgi study. *Pediatric Neurology*, *4*(2), 87–92. https://doi.org/10.1016/0887-8994(88)90047-1

Jahncke, J. N., & Wright, K. M. (2023). The many roles of dystroglycan in nervous system development and function. *Developmental Dynamics*, *252*(1), 61–80. https://doi.org/10.1002/dvdy.516

Kadiyala, S. B., Yannix, J. Q., Nalwalk, J. W., Papandrea, D., Beyer, B. S., Herron, B. J., & Ferland, R. J. (2016). Eight Flurothyl-Induced Generalized Seizures Lead to the Rapid Evolution of Spontaneous Seizures in Mice: A Model of Epileptogenesis with Seizure Remission. *Journal of Neuroscience*, *36*(28), 7485–7496. https://doi.org/10.1523/JNEUROSCI.3232-14.2016

Kanagawa, M. (2021). Dystroglycanopathy: From Elucidation of Molecular and Pathological Mechanisms to Development of Treatment Methods. *International Journal of Molecular Sciences*, *22*(23), Article 23. https://doi.org/10.3390/ijms222313162

Katona, I., Rancz, E. A., Acsady, L., Ledent, C., Mackie, K., Hajos, N., & Freund, T. F. (2001). Distribution of CB1 cannabinoid receptors in the amygdala and their role

in the control of GABAergic transmission. *The Journal of Neuroscience: The Official Journal of the Society for Neuroscience*, *21*(23), 9506–9518. https://doi.org/10.1523/JNEUROSCI.21-23-09506.2001

Knuesel, I., Mastrocola, M., Zuellig, R. A., Bornhauser, B., Schaub, M. C., & Fritschy, J. M. (1999). Altered synaptic clustering of GABAA receptors in mice lacking dystrophin (mdx mice). *European Journal of Neuroscience*, *11*(12), 4457–4462. https://doi.org/10.1046/j.1460-9568.1999.00887.x

Krasowska, E., Zabłocki, K., Górecki, D. C., & Swinny, J. D. (2014). Aberrant location of inhibitory synaptic marker proteins in the hippocampus of dystrophin-deficient mice: Implications for cognitive impairment in Duchenne muscular dystrophy. *PLoS ONE*, *9*(9), e108364. https://doi.org/10.1371/journal.pone.0108364

Larsen, I. S. B., Narimatsu, Y., Joshi, H. J., Yang, Z., Harrison, O. J., Brasch, J., Shapiro, L., Honig, B., Vakhrushev, S. Y., Clausen, H., & Halim, A. (2017). Mammalian O-mannosylation of cadherins and plexins is independent of protein O-mannosyltransferases 1 and 2. *Journal of Biological Chemistry*, *292*(27), 11586–11598. https://doi.org/10.1074/jbc.M117.794487

Lévi, S., Grady, R. M., Henry, M. D., Campbell, K. P., Sanes, J. R., & Craig, A. M. (2002). Dystroglycan Is Selectively Associated with Inhibitory GABAergic Synapses but Is Dispensable for Their Differentiation. *Journal of Neuroscience*, *22*(11), 4274–4285. https://doi.org/10.1523/jneurosci.22-11-04274.2002

Liang, H., Hippenmeyer, S., & Ghashghaei, H. T. (2012). A Nestin-cre transgenic mouse is insufficient for recombination in early embryonic neural progenitors. *Biology Open*, *1*(12), 1200–1203. https://doi.org/10.1242/bio.20122287

Lin, P.-Y., Chen, L. Y., Jiang, M., Trotter, J. H., Seigneur, E., & Südhof, T. C. (2023). Neurexin-2: An inhibitory neurexin that restricts excitatory synapse formation in the hippocampus. *Science Advances*, *9*(1), eadd8856. https://doi.org/10.1126/sciadv.add8856

Lindenmaier, L. B., Parmentier, N., Guo, C., Tissir, F., & Wright, K. M. (2019). Dystroglycan is a scaffold for extracellular axon guidance decisions. *eLife*, *8*. https://doi.org/10.7554/eLife.42143

Manya, H., Chiba, A., Yoshida, A., Wang, X., Chiba, Y., Jigami, Y., Margolis, R. U., & Endo, T. (2004). Demonstration of mammalian protein O-mannosyltransferase activity: Coexpression of POMT1 and POMT2 required for enzymatic activity. *Proceedings of the National Academy of Sciences*, *101*(2), 500–505. https://doi.org/10.1073/pnas.0307228101

Meilleur, K. G., Zukosky, K., Medne, L., Fequiere, P., Powell-Hamilton, N., Winder, T. L., Alsaman, A., El-Hattab, A. W., Dastgir, J., Hu, Y., Donkervoort, S., Golden, J. A., Eagle, R., Finkel, R., Scavina, M., Hood, I. C., Rorke-Adams, L. B., & Bönnemann, C. G. (2014). Clinical, pathologic, and mutational spectrum of dystroglycanopathy caused by LARGE mutations. *Journal of Neuropathology and Experimental Neurology*, *73*(5), 425–441. https://doi.org/10.1097/NEN.0000000000000065

Menezes, M. J., McClenahan, F. K., Leiton, C. V., Aranmolate, A., Shan, X., & Colognato, H. (2014). The extracellular matrix protein laminin α2 regulates the maturation and function of the blood–brain barrier. *Journal of Neuroscience*, *34*(46), 15260–15280. https://doi.org/10.1523/JNEUROSCI.3678-13.2014

Mercuri, E., Messina, S., Bruno, C., Mora, M., Pegoraro, E., Comi, G. P., D'Amico, A., Aiello, C., Biancheri, R., Berardinelli, A., Boffi, P., Cassandrini, D., Laverda, A., Moggio, M., Morandi, L., Moroni, I., Pane, M., Pezzani, R., Pichiecchio, A., … Bertini, E. (2009). Congenital muscular dystrophies with defective glycosylation of dystroglycan: A population study. *Neurology*, *72*(21), 1802–1809. https://doi.org/10.1212/01.wnl.0000346518.68110.60

Miczán, V., Kelemen, K., Glavinics, J. R., László, Z. I., Barti, B., Kenesei, K., Kisfali, M., & Katona, I. (2021). NECAB1 and NECAB2 are Prevalent Calcium-Binding Proteins of CB1/CCK-Positive GABAergic Interneurons. *Cerebral Cortex*, *31*(3), 1786–1806. https://doi.org/10.1093/cercor/bhaa326

Miller, D. S., & Wright, K. M. (2021). Neuronal Dystroglycan regulates postnatal development of CCK/cannabinoid receptor-1 interneurons. *Neural Development*, *16*(1). https://doi.org/10.1186/s13064-021-00153-1

Missler, M., Zhang, W., Rohlmann, A., Kattenstroth, G., Hammer, R. E., Gottmann, K., & Südhof, T. C. (2003). α-Neurexins couple Ca2+ channels to synaptic vesicle exocytosis. *Nature*, *423*(6943), Article 6943. https://doi.org/10.1038/nature01755

Moizard, M.-P., Toutain, A., Fournier, D., Berret, F., Raynaud, M., Billard, C., Andres, C., & Moraine, C. (2000). Severe cognitive impairment in DMD: Obvious clinical evidence for Dp71 isoform point mutations screening. *European Journal of Human Genetics*, *8*(7), Article 7. https://doi.org/10.1038/sj.ejhg.5200488

Monory, K., Polack, M., Remus, A., Lutz, B., & Korte, M. (2015). Cannabinoid CB1 Receptor Calibrates Excitatory Synaptic Balance in the Mouse Hippocampus.

Journal of Neuroscience, *35*(9), 3842–3850. https://doi.org/10.1523/JNEUROSCI.3167-14.2015

Moore, C. J., & Winder, S. J. (2010). Dystroglycan versatility in cell adhesion: A tale of multiple motifs. *Cell Communication and Signaling*, *8*(1), 3. https://doi.org/10.1186/1478-811X-8-3

Moore, S. A., Saito, F., Chen, J., Michele, D. E., Henry, M. D., Messing, A., Cohn, R. D., Ross-Barta, S. E., Westra, S., Williamson, R. A., Hosl, T., & Campbell, K. P. (2002). Deletion of brain dystroglycan recapitulates aspects of congenital muscular dystrophy. *Nature*, *418*(6896), 422–425. https://doi.org/10.1038/nature00838

Morozov, Y. M., & Freund, T. F. (2003a). Postnatal development and migration of cholecystokinin-immunoreactive interneurons in rat hippocampus. *Neuroscience*, *120*(4), 923–939. https://doi.org/10.1016/S0306-4522(03)00409-3

Morozov, Y. M., & Freund, T. F. (2003b). Post-natal development of type 1 cannabinoid receptor immunoreactivity in the rat hippocampus. *The European Journal of Neuroscience*, *18*(5), 1213–1222. https://doi.org/10.1046/j.1460-9568.2003.02852.x

Morozov, Y. M., Torii, M., & Rakic, P. (2009). Origin, Early Commitment, Migratory Routes, and Destination of Cannabinoid Type 1 Receptor-Containing Interneurons. *Cerebral Cortex*, *19*(suppl_1), i78–i89. https://doi.org/10.1093/cercor/bhp028

Mulder, J., Aguado, T., Keimpema, E., Barabás, K., Ballester Rosado, C. J., Nguyen, L., Monory, K., Marsicano, G., Di Marzo, V., Hurd, Y. L., Guillemot, F., Mackie, K.,

Lutz, B., Guzmán, M., Lu, H.-C., Galve-Roperh, I., & Harkany, T. (2008). Endocannabinoid signaling controls pyramidal cell specification and long-range axon patterning. *Proceedings of the National Academy of Sciences*, *105*(25), 8760–8765. https://doi.org/10.1073/pnas.0803545105

Muntoni, F., Torelli, S., Wells, D. J., & Brown, S. C. (2011). Muscular dystrophies due to glycosylation defects: Diagnosis and therapeutic strategies. *Current Opinion in Neurology*, *24*(5), 437–442. https://doi.org/10.1097/WCO.0b013e32834a95e3

Myshrall, T. D., Moore, S. A., Ostendorf, A. P., Satz, J. S., Kowalczyk, T., Nguyen, H., Daza, R. A. M., Lau, C., Campbell, K. P., & Hevner, R. F. (2012). Dystroglycan on radial glia end feet is required for pial basement membrane integrity and columnar organization of the developing cerebral cortex. *Journal of Neuropathology and Experimental Neurology*, *71*(12), 1047–1063. https://doi.org/10.1097/NEN.0b013e318274a128

Nagode, D. A., Tang, A.-H., Yang, K., & Alger, B. E. (2014). Optogenetic identification of an intrinsic cholinergically driven inhibitory oscillator sensitive to cannabinoids and opioids in hippocampal CA1. *The Journal of Physiology*, *592*(Pt 1), 103–123. https://doi.org/10.1113/jphysiol.2013.257428

Naidoo, M., & Anthony, K. (2020). Dystrophin Dp71 and the Neuropathophysiology of Duchenne Muscular Dystrophy. *Molecular Neurobiology*, *57*(3), 1748–1767. https://doi.org/10.1007/s12035-019-01845-w

Nguyen, H., Ostendorf, A. P., Satz, J. S., Westra, S., Ross-Barta, S. E., Campbell, K. P., & Moore, S. A. (2014). Glial scaffold required for cerebellar granule cell migration is dependent on dystroglycan function as a receptor for basement

membrane proteins. *Acta Neuropathologica Communications*, *2*(1). https://doi.org/10.1186/2051-5960-1-58

Nickolls, A. R., & Bönnemann, C. G. (2018). The roles of dystroglycan in the nervous system: Insights from animal models of muscular dystrophy. *DMM Disease Models and Mechanisms*, *11*(12), dmm035931. https://doi.org/10.1242/dmm.035931

Omori, Y., Araki, F., Chaya, T., Kajimura, N., Irie, S., Terada, K., Muranishi, Y., Tsujii, T., Ueno, S., Koyasu, T., Tamaki, Y., Kondo, M., Amano, S., & Furukawa, T. (2012). Presynaptic dystroglycan-pikachurin complex regulates the proper synaptic connection between retinal photoreceptor and bipolar cells. *Journal of Neuroscience*, *32*(18), 6126–6137. https://doi.org/10.1523/JNEUROSCI.0322-12.2012

Orlandi, C., Omori, Y., Wang, Y., Cao, Y., Ueno, A., Roux, M. J., Condomitti, G., de Wit, J., Kanagawa, M., Furukawa, T., & Martemyanov, K. A. (2018). Transsynaptic Binding of Orphan Receptor GPR179 to Dystroglycan-Pikachurin Complex Is Essential for the Synaptic Organization of Photoreceptors. *Cell Reports*, *25*(1), 130-145.e5. https://doi.org/10.1016/j.celrep.2018.08.068

Patrizi, A., Scelfo, B., Viltono, L., Briatore, F., Fukaya, M., Watanabe, M., Strata, P., Varoqueaux, F., Brose, N., Fritschy, J.-M., & Sassoè-Pognetto, M. (2008). Synapse formation and clustering of neuroligin-2 in the absence of GABAA receptors. *Proceedings of the National Academy of Sciences*, *105*(35), 13151–13156. https://doi.org/10.1073/pnas.0802390105

Pawlisz, A. S., & Feng, Y. (2011). Three-dimensional regulation of radial glial functions by lis1-nde1 and dystrophin glycoprotein complexes. *PLoS Biology*, *9*(10). https://doi.org/10.1371/journal.pbio.1001172

Peron, S. P., Freeman, J., Iyer, V., Guo, C., & Svoboda, K. (2015). A Cellular Resolution Map of Barrel Cortex Activity during Tactile Behavior. *Neuron*, *86*(3), 783–799. https://doi.org/10.1016/j.neuron.2015.03.027

Raphael, A. R., Couthouis, J., Sakamuri, S., Siskind, C., Vogel, H., Day, J. W., & Gitler, A. D. (2014). Congenital Muscular Dystrophy and Generalized Epilepsy Caused by GMPPB Mutations. *Brain Research*, *0*, 66–71. https://doi.org/10.1016/j.brainres.2014.04.028

Reeuwijk, J. van, Janssen, M., Elzen, C. van den, Bernabé, D. B.-V. de, Sabatelli, P., Merlini, L., Boon, M., Scheffer, H., Brockington, M., Muntoni, F., Huynen, M. A., Verrips, A., Walsh, C. A., Barth, P. G., Brunner, H. G., & Bokhoven, H. van. (2005). POMT2 mutations cause α-dystroglycan hypoglycosylation and Walker-Warburg syndrome. *Journal of Medical Genetics*, *42*(12), 907–912. https://doi.org/10.1136/jmg.2005.031963

Reissner, C., Stahn, J., Breuer, D., Klose, M., Pohlentz, G., Mormann, M., & Missler, M. (2014). Dystroglycan binding to α-Neurexin competes with neurexophilin-1 and neuroligin in the brain. *Journal of Biological Chemistry*, *289*(40), 27585–27603. https://doi.org/10.1074/jbc.M114.595413

Rubio-Fernández, M., Uribe, M. L., Vicente-Tejedor, J., Germain, F., Susín-Lara, C., Quereda, C., Montoliu, L., de la Villa, P., Martín-Nieto, J., & Cruces, J. (2018). Impairment of photoreceptor ribbon synapses in a novel Pomt1 conditional

knockout mouse model of dystroglycanopathy. *Scientific Reports*, *8*(1), Article 1. https://doi.org/10.1038/s41598-018-26855-x

Satz, J. S., Barresi, R., Durbeej, M., Willer, T., Turner, A., Moore, S. A., & Campbell, K. P. (2008). Brain and eye malformations resembling Walker-Warburg syndrome are recapitulated in mice by dystroglycan deletion in the epiblast. *Journal of Neuroscience*, *28*(42), 10567–10575. https://doi.org/10.1523/JNEUROSCI.2457-08.2008

Satz, J. S., Ostendorf, A. P., Hou, S., Turner, A., Kusano, H., Lee, J. C., Turk, R., Nguyen, H., Ross-Barta, S. E., Westra, S., Hoshi, T., Moore, S. A., & Campbell, K. P. (2010). Distinct functions of glial and neuronal dystroglycan in the developing and adult mouse brain. *Journal of Neuroscience*, *30*(43), 14560–14572. https://doi.org/10.1523/JNEUROSCI.3247-10.2010

Satz, J. S., Philp, A. R., Nguyen, H., Kusano, H., Lee, J., Turk, R., Riker, M. J., Hernández, J., Weiss, R. M., Anderson, M. G., Mullins, R. F., Moore, S. A., Stone, E. M., & Campbell, K. P. (2009). Visual impairment in the absence of dystroglycan. *Journal of Neuroscience*, *29*(42), 13136–13146. https://doi.org/10.1523/JNEUROSCI.0474-09.2009

Schindelin, J., Arganda-Carreras, I., Frise, E., Kaynig, V., Longair, M., Pietzsch, T., Preibisch, S., Rueden, C., Saalfeld, S., Schmid, B., Tinevez, J.-Y., White, D. J., Hartenstein, V., Eliceiri, K., Tomancak, P., & Cardona, A. (2012). Fiji: An open-source platform for biological-image analysis. *Nature Methods*, *9*(7), Article 7. https://doi.org/10.1038/nmeth.2019

Sheikh, M. O., Capicciotti, C. J., Liu, L., Praissman, J., Ding, D., Mead, D. G., Brindley, M. A., Willer, T., Campbell, K. P., Moremen, K. W., Wells, L., & Boons, G.-J. (2022). Cell surface glycan engineering reveals that matriglycan alone can recapitulate dystroglycan binding and function. *Nature Communications*, *13*(1), Article 1. https://doi.org/10.1038/s41467-022-31205-7

Südhof, T. C. (2018). Towards an Understanding of Synapse Formation. *Neuron*, *100*(2), 276–293. https://doi.org/10.1016/j.neuron.2018.09.040

Sugita, S., Saito, F., Tang, J., Satz, J., Campbell, K., & Südhof, T. C. (2001). A stoichiometric complex of neurexins and dystroglycan in brain. *Journal of Cell Biology*, *154*(2), 435–445. https://doi.org/10.1083/jcb.200105003

Taniguchi-Ikeda, M., Morioka, I., Iijima, K., & Toda, T. (2016). Mechanistic aspects of the formation of α-dystroglycan and therapeutic research for the treatment of α-dystroglycanopathy: A review. *Molecular Aspects of Medicine*, *51*, 115–124. https://doi.org/10.1016/j.mam.2016.07.003

Tian, M., Jacobson, C., Gee, S. H., Campbell, K. P., Carbonetto, S., & Jucker, M. (1996). Dystroglycan in the cerebellum is a laminin α2-chain binding protein at the glial-vascular interface and is expressed in Purkinje cells. *European Journal of Neuroscience*, *8*(12), 2739–2747. https://doi.org/10.1111/j.1460-9568.1996.tb01568.x

Tronche, F., Kellendonk, C., Kretz, O., Gass, P., Anlag, K., Orban, P. C., Bock, R., Klein, R., & Schütz, G. (1999). Disruption of the glucocorticoid receptor gene in the nervous system results in reduced anxiety. *Nature Genetics*, *23*(1), Article 1. https://doi.org/10.1038/12703

Trotter, J. H., Wang, C. Y., Zhou, P., Nakahara, G., & Südhof, T. C. (2023). A combinatorial code of neurexin-3 alternative splicing controls inhibitory synapses via a trans-synaptic dystroglycan signaling loop. *Nature Communications*, *14*(1), Article 1. https://doi.org/10.1038/s41467-023-36872-8

Uezu, A., Hisey, E., Kobayashi, Y., Gao, Y., Bradshaw, T. W. A., Devlin, P., Rodriguiz, R., Tata, P. R., & Soderling, S. H. (2019). Essential role for insyn1 in dystroglycan complex integrity and cognitive behaviors in mice. *eLife*, *8*. https://doi.org/10.7554/eLife.50712

Ullrich, B., Ushkaryov, Y. A., & Südhof, T. C. (1995). Cartography of neurexins: More than 1000 isoforms generated by alternative splicing and expressed in distinct subsets of neurons. *Neuron*, *14*(3), 497–507. https://doi.org/10.1016/0896-6273(95)90306-2

Vitalis, T., Lainé, J., Simon, A., Roland, A., Leterrier, C., & Lenkei, Z. (2008). The type 1 cannabinoid receptor is highly expressed in embryonic cortical projection neurons and negatively regulates neurite growth in vitro. *European Journal of Neuroscience*, *28*(9), 1705–1718. https://doi.org/10.1111/j.1460-9568.2008.06484.x

Wang, J., Lin, Z.-J., Liu, L., Xu, H.-Q., Shi, Y.-W., Yi, Y.-H., He, N., & Liao, W.-P. (2017). Epilepsy-associated genes. *Seizure*, *44*, 11–20. https://doi.org/10.1016/j.seizure.2016.11.030

Willer, T., Inamori, K., Venzke, D., Harvey, C., Morgensen, G., Hara, Y., Beltrán Valero de Bernabé, D., Yu, L., Wright, K. M., & Campbell, K. P. (2014). The glucuronyltransferase B4GAT1 is required for initiation of LARGE-mediated α-

dystroglycan functional glycosylation. *eLife*, *3*, e03941. https://doi.org/10.7554/eLife.03941

Wright, K. M., Lyon, K. A., Leung, H., Leahy, D. J., Ma, L., & Ginty, D. D. (2012). Dystroglycan Organizes Axon Guidance Cue Localization and Axonal Pathfinding. *Neuron*, *76*(5), 931–944. https://doi.org/10.1016/j.neuron.2012.10.009

Yanagisawa, A., Bouchet, C., Bergh, P. Y. K. V. den, Cuisset, J.-M., Viollet, L., Leturcq, F., Romero, N. B., Quijano-Roy, S., Fardeau, M., Seta, N., & Guicheney, P. (2007). New POMT2 mutations causing congenital muscular dystrophy: Identification of a founder mutation. *Neurology*, *69*(12), 1254–1260. https://doi.org/10.1212/01.wnl.0000268489.60809.c4

Yang, H., Song, D., Liu, Y., Chen, X., Zhu, Y., Wei, C., Fu, X., Liu, X., Yang, Z., & Xiong, H. (2022). Seizures and EEG characteristics in a cohort of pediatric patients with dystroglycanopathies. *Seizure*, *101*, 39–47. https://doi.org/10.1016/j.seizure.2022.07.008

Yoshida-Moriguchi, T., & Campbell, K. P. (2015). Matriglycan: A novel polysaccharide that links dystroglycan to the basement membrane. *Glycobiology*, *25*(7), 702–713. https://doi.org/10.1093/glycob/cwv021

Zaccaria, M. L., Di Tommaso, F., Brancaccio, A., Paggi, P., & Petrucci, T. C. (2001). Dystroglycan distribution in adult mouse brain: A light and electron microscopy study. *Neuroscience*, *104*(2), 311–324. https://doi.org/10.1016/S0306-4522(01)00092-6

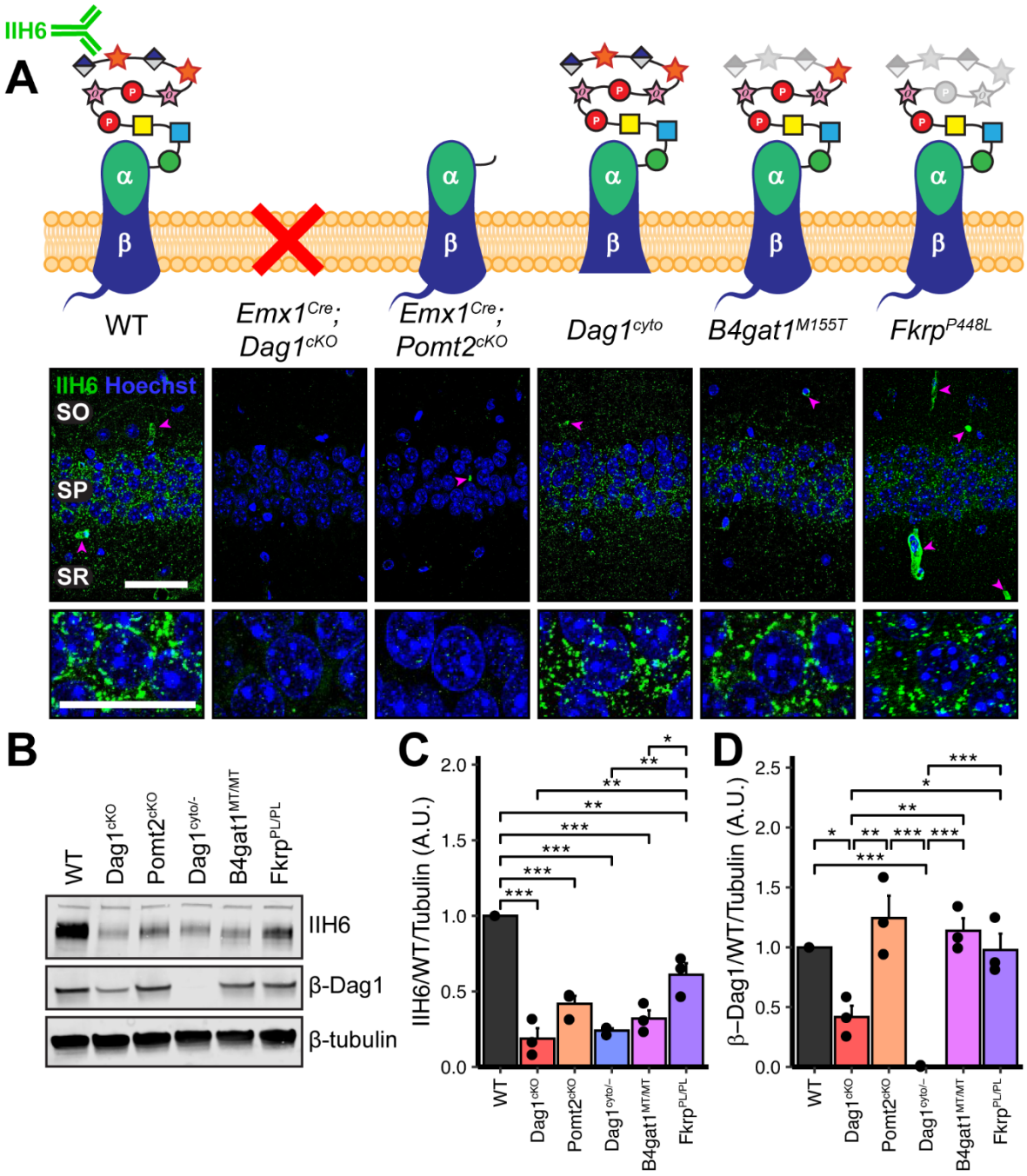

Figure 1. Dystroglycan synaptic localization and glycosylation in mouse models of dystroglycanopathy. (A) Schematic depiction of Dystroglycan in different mouse models. The IIH6 antibody recognizes the matriglycan repeats on extracellular αDag1. Hippocampal CA1 of P30 mice immunostained for Dystroglycan glycosylation (IIH6, green) and nuclear marker Hoechst (blue) show puncta of glycosylated Dystroglycan localized to the perisomatic region of pyramidal cells and to blood vessels (magenta arrowheads); scale bar = 50μm. Lower panels show cell bodies in SP; scale bar = 25μm. CA1 layers: SO, *stratum oriens*; SP, *stratum pyramidale*; SR, *stratum radiatum*.

(B) WGA-enriched lysates from P0 forebrain were immunoblotted for IIH6, β-Dag1, and β-tubulin. **(C-D)** Quantification of immunoblot in **(B)**. Error bars show mean + SEM.

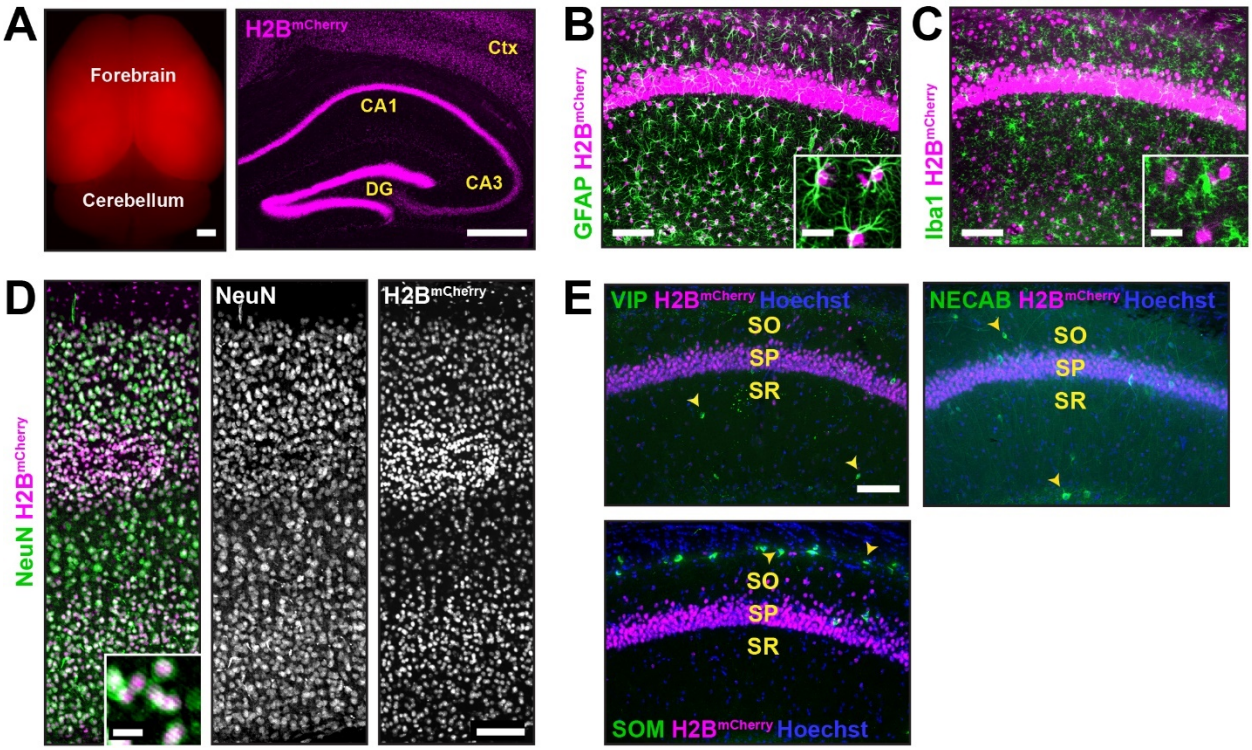

Figure 1 Supplement 1. *Emx1^{Cre}* drives recombination in forebrain excitatory neurons and astrocytes, but not interneurons or microglia. (A) Left; endogenous red fluorescence in the forebrain of P60 *Emx1^{Cre}*;*R26$^{LSL\text{-}H2B\text{-}mCherry}$* reporter mice (scale bar = 1mm). Right; coronal section of the forebrain from *Emx1^{Cre}*;*R26$^{LSL\text{-}H2B\text{-}mCherry}$* mice showing robust nuclear mCherry signal (magenta) in the cortex and hippocampus (scale bar = 500μm). **(B-E)** mCherry^{+} nuclei shown with markers of multiple cell types in the brain including astrocytes (GFAP, green) **(B)**, microglia (Iba1, green) **(C)**, and neurons (NeuN, green) **(D)** (scale bar = 100μm). Insets show enlarged images of mCherry^{+} nuclei with cell type markers (scale bar = 20μm). **(E)** mCherry^{+} nuclei with markers for different interneuron subtype markers (yellow arrowheads) (scale bar = 100μm) (VIP = Vasoactive intestinal peptide, NECAB = Neuronal calcium-binding protein 1, SOM = Somatostatin). *CA1 layers: SO, stratum oriens; SP, stratum pyramidale; SR, stratum radiatum.*

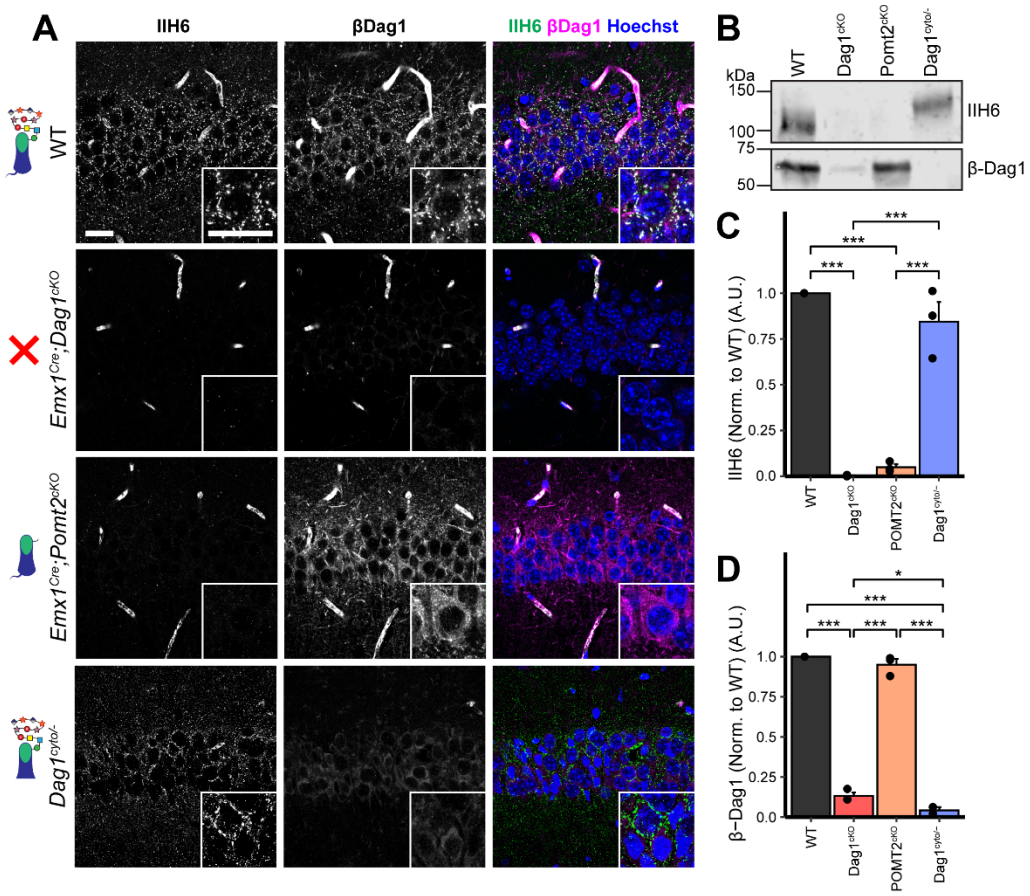

Figure 1 Supplement 2. Dystroglycan glycosylation is required for synaptic localization. (A) Immunostaining for matriglycan (IIH6, green) and β-Dag1 (magenta) in CA1 pyramidal cells of WT controls, *Emx1^{Cre};Dag1^{cKOs}*, *Emx1^{Cre};Pomt2^{cKOs}*, and *Dag1$^{cyto/-}$* mutants. Scale bars = 25μm. **(B)** WGA-enriched lysates from P21-P30 hippocampus were immunoblotted for IIH6 and β-Dag1. **(C-D)** Quantification of immunoblot in **(B)**. Error bars show mean + SEM.

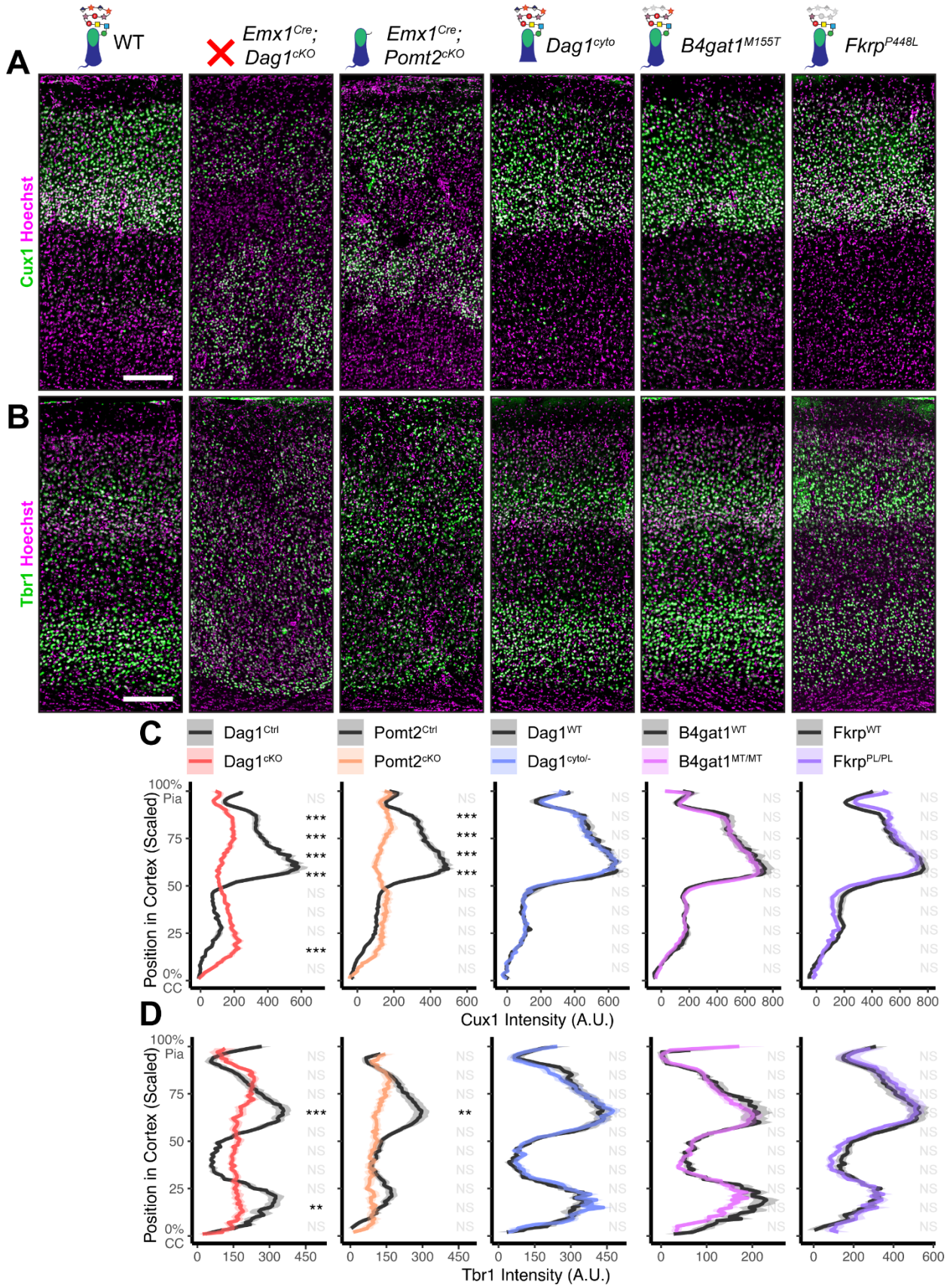
A
WT
Emx1Cre; Dag1cKO
Emx1Cre; Pomt2cKO
Dag1cyto
B4gat1M155T
FkrpP448L
Cux1 Hoechst
B
Tbr1 Hoechst
C
Dag1Ctrl
Dag1cKO
Pomt2Ctrl
Pomt2cKO
Dag1WT
Dag1cyto/-
B4gat1WT
B4gat1MT/MT
FkrpWT
FkrpPL/PL
Position in Cortex (Scaled)
100% Pia
75
50
25
0% CC
Cux1 Intensity (A.U.)
D
Tbr1 Intensity (A.U.)

Figure 2. Dystroglycan is required for cortical neuron migration in a glycosylation-dependent manner and independent of intracellular interactions. Immunostaining for cortical layer markers **(A)** Cux1 (layers 2-4) and **(B)** Tbr1 (layers 3 and 6) in P30 somatosensory cortex (scale bar = 200μm). Layer markers are shown in green. Nuclear marker Hoechst is shown in magenta. Quantification of fluorescence intensity of layer markers shown for **(C)** Cux1 and **(D)** Tbr1**.** Shaded regions of intensity profile illustrate ± SEM. See **Supplementary Table 1** for Ns. *Significance: * = $p < 0.05$, ** = $p < 0.01$, *** = $p < 0.001$, NS = $p \geq 0.05$. Abbreviations: CC, corpus callosum; A.U., arbitrary units.*

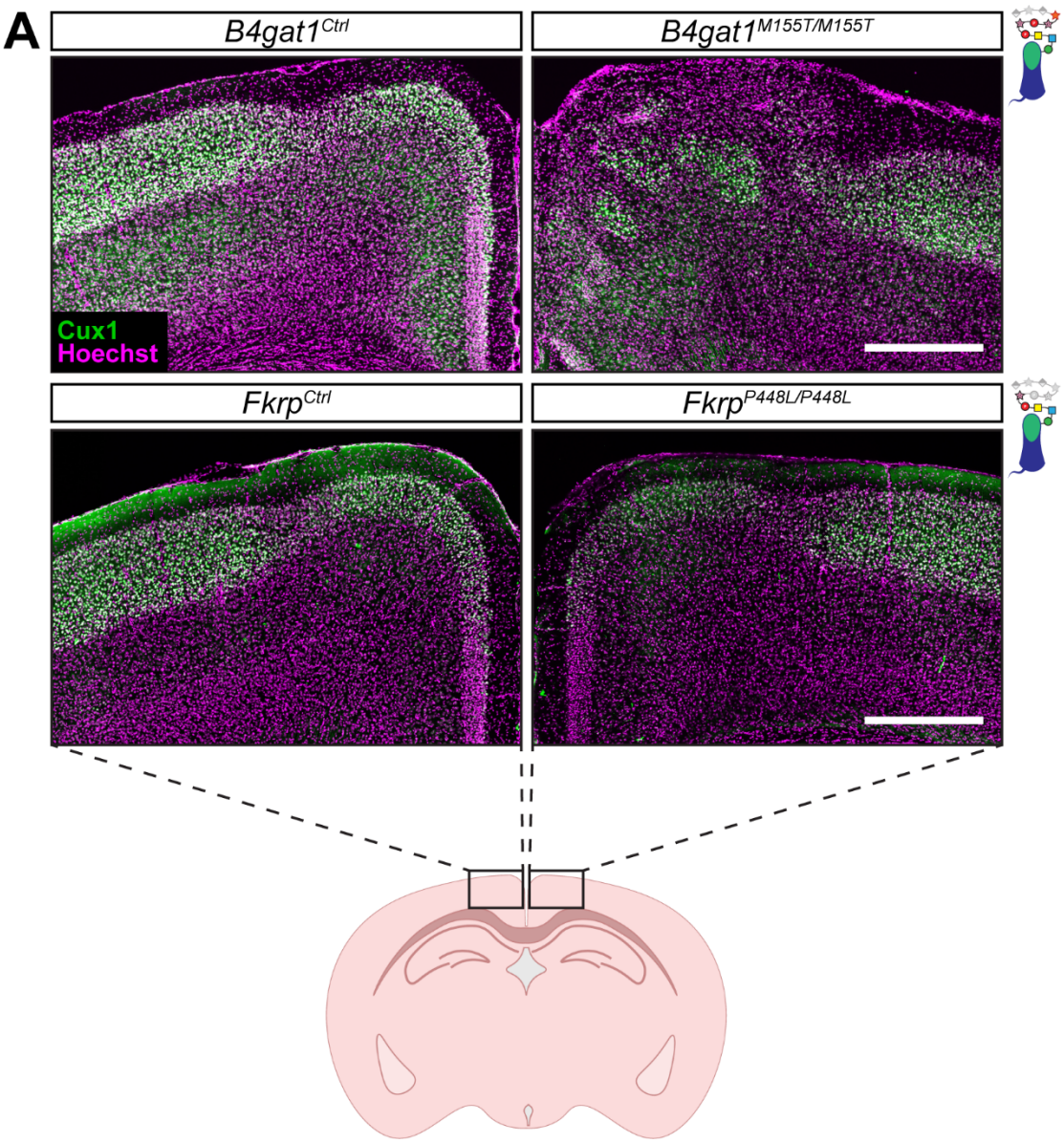

Figure 2 Supplement 1. Cortical migration is disrupted at midline of *B4gat1*$^{M155T/M155T}$ but not *Fkrp*$^{P448L/P448L}$ mutants. (A) Immunostaining for cortical layer marker Cux1 (layers 2-4) in P30 somatosensory cortex (scale bar = 500µm). Cux1 is shown in green. Nuclear marker Hoechst is shown in magenta. Cortical migration is normal in both *B4gat1* and *Fkrp* point mutants except at midline, where the *B4gat1* mutants show a migration phenotype not seen in the *Fkrp* point mutants. This phenotype was observed with 100% penetrance in the *B4gat1* mutants and 0% in the *Fkrp* mutants.

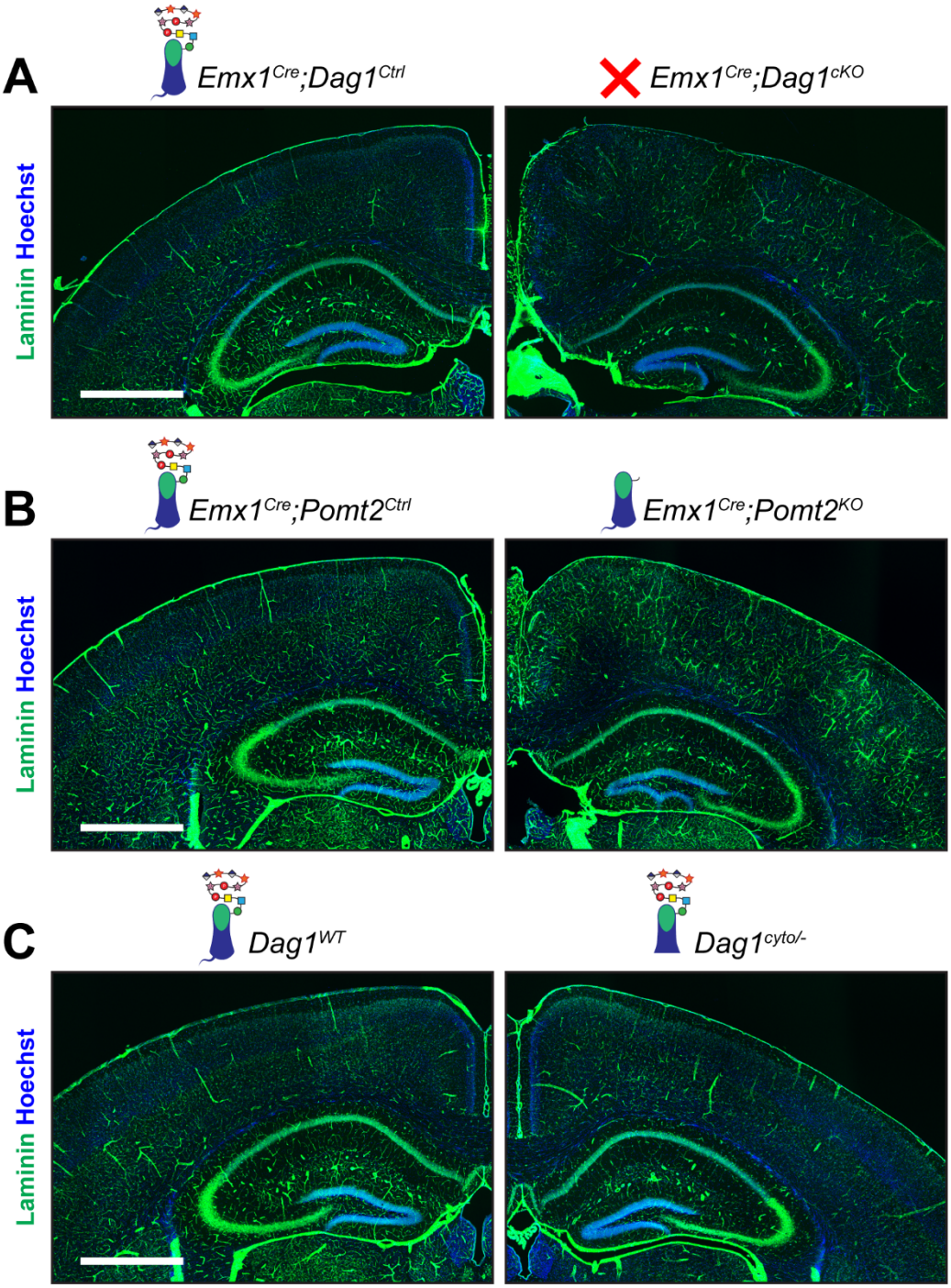

Figure 2 Supplement 2. Laminin immunoreactivity in adult neocortex appears discontinuous in *Dag1* mutants. (A-C) Immunostaining for ECM protein Laminin (green). Nuclear marker Hoechst is shown in blue. Scale bar = 1000μm.

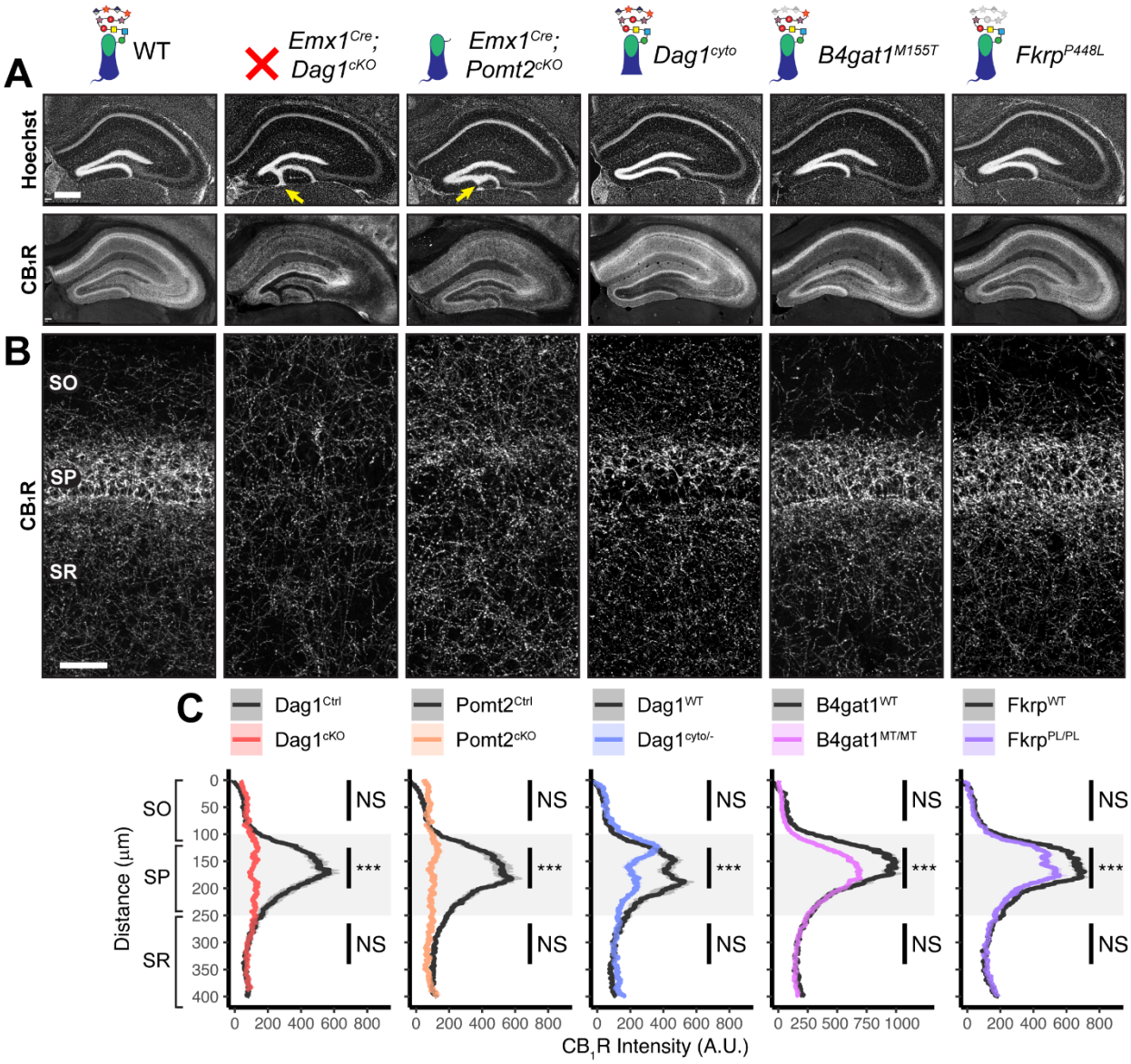

Figure 3. *Dag1* is required for CCK⁺/CB₁R⁺ basket IN perisomatic axon targeting in *stratum pyramidale* of hippocampal CA1-3. (A) Nuclear marker Hoechst (upper panels) shows hippocampal morphology. Granule cell migration is disrupted in dentate gyrus of *Emx1^{Cre};Dag1^{cKOs}* and *Emx1^{Cre};POMT2^{cKOs}* (yellow arrows). CA1-3 gross morphology is normal in all models. CB_1R immunostaining (lower panels) shows abnormal CCK^+/CB_1R^+ basket interneuron targeting in CA1-3 to varying degrees across models (scale bar = 400µm). **(B)** Higher magnification view of CB_1R immunostaining in CA1 (scale bar = 50µm). **(C)** Quantification of CA1 CB_1R fluorescence intensity profile. Shaded regions of intensity profile illustrate ± SEM. Gray region highlights SP. See **Supplementary Table 1** for Ns. *Significance: * = $p < 0.05$, ** = $p < 0.01$, *** = $p < 0.001$, NS = $p \geq 0.05$. Abbreviations: A.U., arbitrary units; SO, stratum oriens; SP, stratum pyramidale; SR, stratum radiatum.*

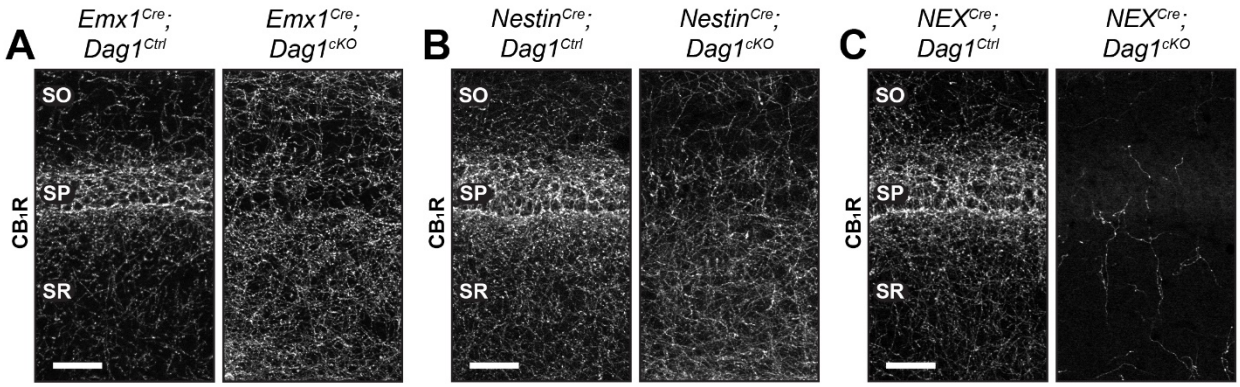

Figure 3 Supplement 1. CCK$^+$/CB$_1$R$^+$ IN axon targeting phenotypes in hippocampal CA1 of various *Dag1^{cKOs}*. CB$_1$R immunostaining in hippocampal CA1 of control mice (left panels) and *Dag1^{cKOs}* (right panels) generated using *Emx1^{Cre}* (forebrain progenitors, E10.5) **(A)**, *Nestin^{Cre}* (neural stem cells in the central and peripheral nervous systems, E11.5) **(B)**, and *NEX^{Cre}* (forebrain postmitotic excitatory neurons, E12.5) **(C)**. Scale bar = 50µm. *Abbreviations: SO, stratum oriens; SP, stratum pyramidale; SR, stratum radiatum.*

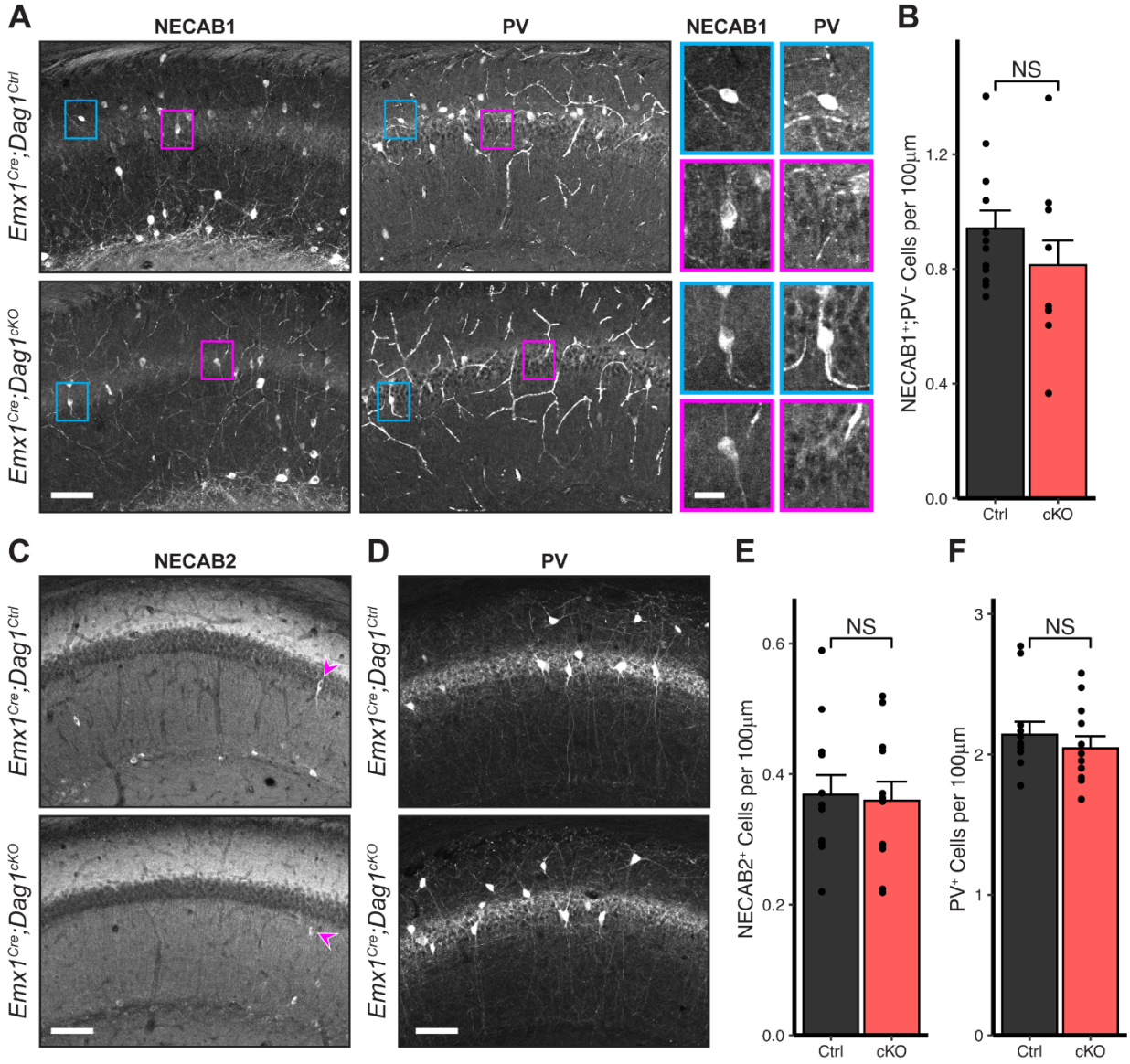

Figure 3 Supplement 2. CCK⁺/CB₁R⁺ IN cell numbers are unchanged in *Emx1^{Cre};Dag1^{cKOs}*. (A) Immunostaining in hippocampal CA1 for NECAB1 (left) and PV (right) in *Emx1^{Cre};Dag1^{Ctrl}* and *Emx1^{Cre};Dag1^{cKO}* mice. NECAB1 labeling is evident in PV⁺ cells (example shown in blue inset) and in an additional PV⁻ population that contains the CCK⁺/CB₁R⁺ population (example shown in magenta inset). The average number of NECAB1⁺;PV⁻ cells per 100µm of SP is quantified in **(B)**. Immunostaining for NECAB2 **(C)** and PV **(D)** with cell number quantification in **(E)** and **(F)**. Scale bar = 100µm. Error bars show mean + SEM. See **Supplementary Table 1** for Ns. *Significance: * = $p < 0.05$, ** = $p < 0.01$, *** = $p < 0.001$, NS = $p \geq 0.05$. Abbreviations: SP, stratum pyramidale; PV, parvalbumin.*

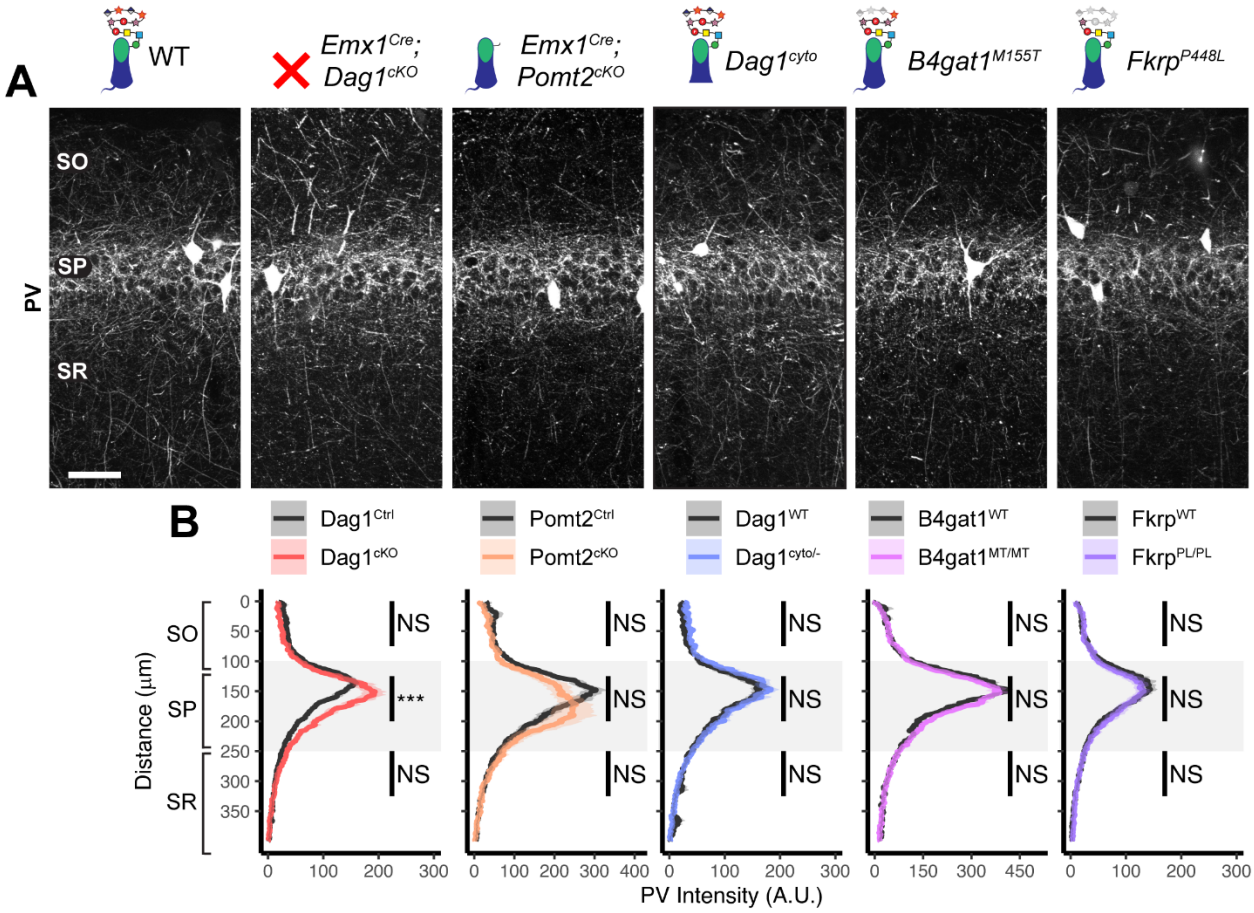

Figure 3 Supplement 3. Parvalbumin⁺ basket INs do not require *Dag1* for proper axon targeting in hippocampal CA1. (A) Parvalbumin (PV) immunostaining in P30 hippocampal CA1 shows that PV⁺ basket interneurons exhibit normal distribution in CA1 for all genetic models except for an increase in PV intensity within *stratum pyramidale* of *Emx1^{Cre};Dag1^{cKOs}* (scale bar = 50µm). **(B)** Quantification of CA1 PV fluorescence intensity profile. Shaded regions of intensity profile illustrate ± SEM. Gray region highlights SP. See **Supplementary Table 1** for Ns. *Significance: * = p < 0.05, ** = p < 0.01, *** = p < 0.001, NS = p ≥ 0.05. Abbreviations: A.U., arbitrary units; SO, stratum oriens; SP, stratum pyramidale; SR, stratum radiatum.*

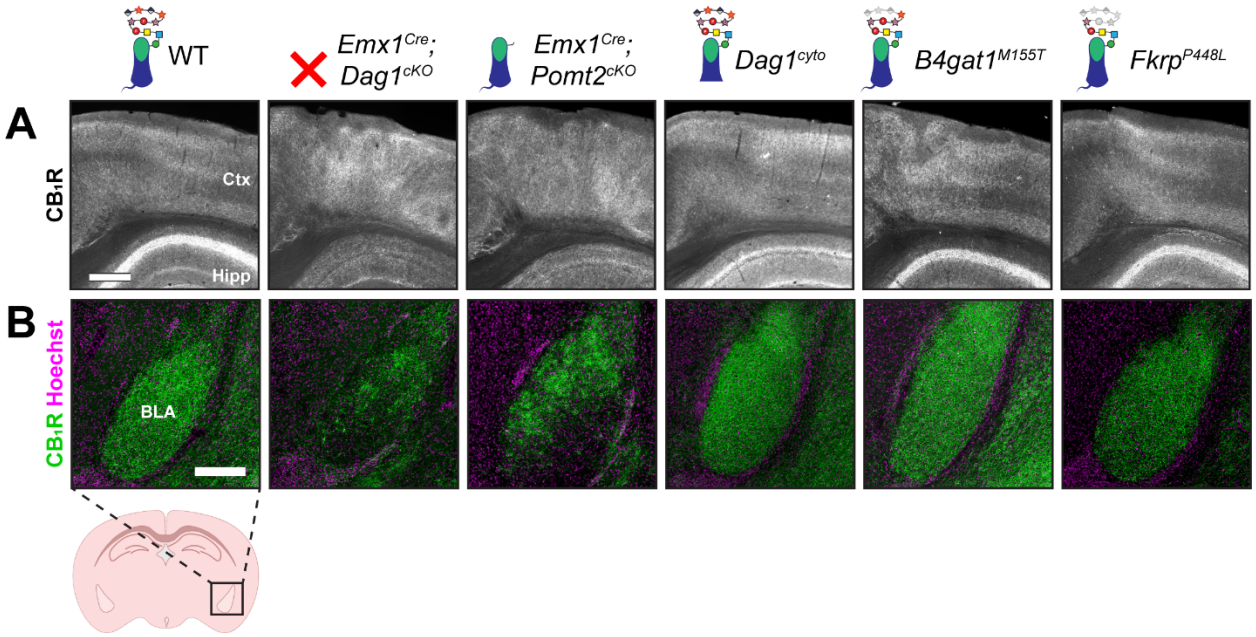

Figure 3 Supplement 4. Altered CB_1R expression in cortex and basolateral amygdala of *Dag1* and *POMT2* mutants. (A) CB_1R immunostaining in P30 coronal sections showing somatosensory cortex (Ctx) and CA1 of hippocampus (Hipp) (scale bar = 400μm). **(B)** CB_1R immunostaining (green) shown with nuclear marker Hoechst (magenta) in basolateral amygdala (BLA) (scale bar = 250μm).

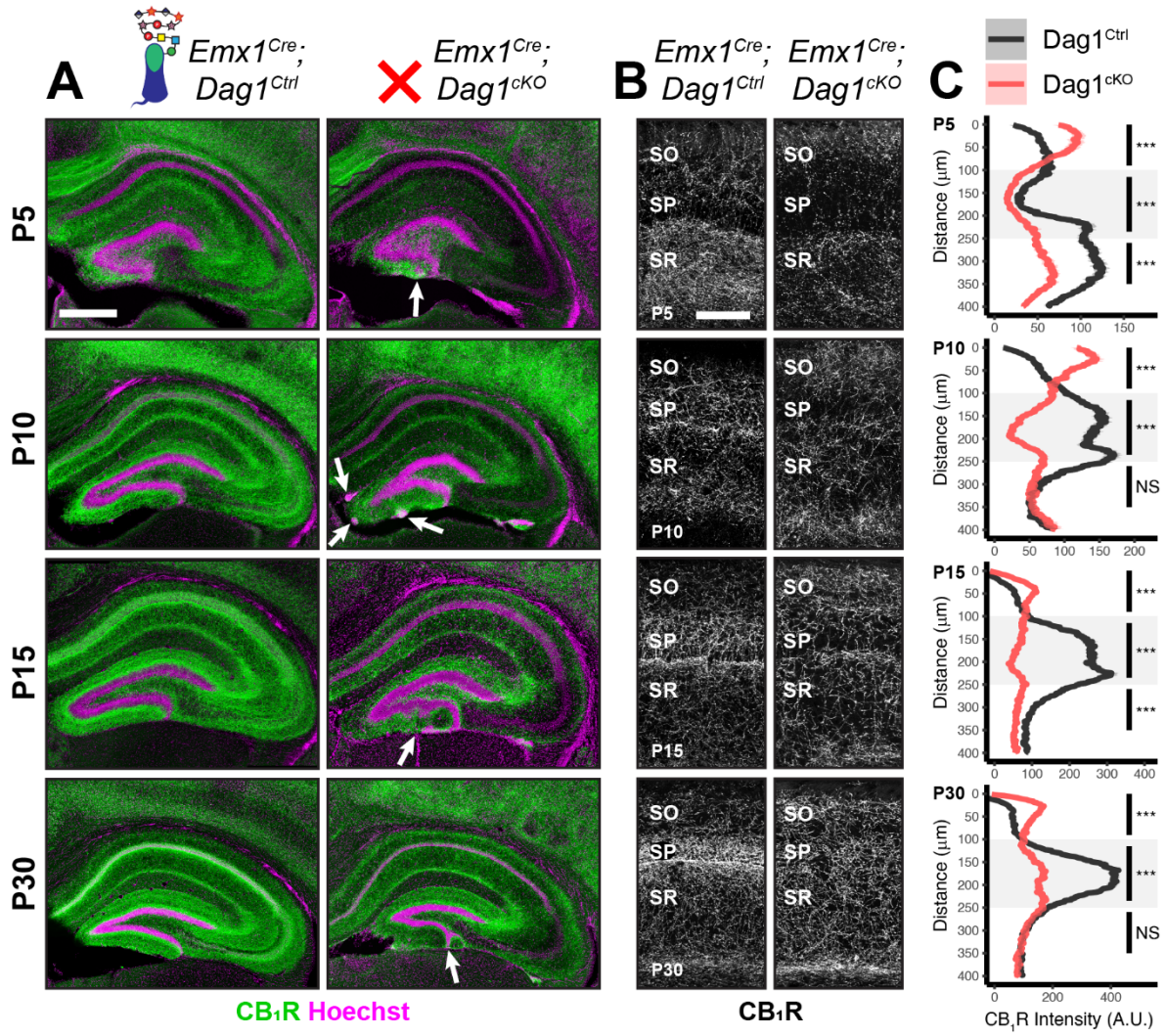

Figure 4. *Dag1* is required for CCK⁺/CB₁R⁺ IN axon targeting during early postnatal development. (A) Immunostaining for CB_1R^+ axon terminals (green) in the hippocampus of *Emx1^{Cre};Dag1* controls (left) and cKOs (right) at ages P5-P30. Nuclear marker Hoechst is shown in magenta. White arrowheads indicate migration errors in dentate granule cells *Emx1^{Cre};Dag1^{cKO}* mice. Scale bar = 500µm. **(B)** Higher magnification images of CB_1R^+ axon terminals in CA1 of *Emx1^{Cre};Dag1* controls (left) and cKOs (right) at ages P5-P30. Scale bar = 100µm. **(C)** Quantification of CB_1R fluorescence intensity profile in CA1. Shaded regions of intensity profile illustrate ± SEM. Gray region highlights SP. See **Supplementary Table 1** for Ns. *Significance:* * = $p < 0.05$, ** = $p < 0.01$, *** = $p < 0.001$, NS = $p \geq 0.05$. *Abbreviations: A.U., arbitrary units; SO, stratum oriens; SP, stratum pyramidale; SR, stratum radiatum.*

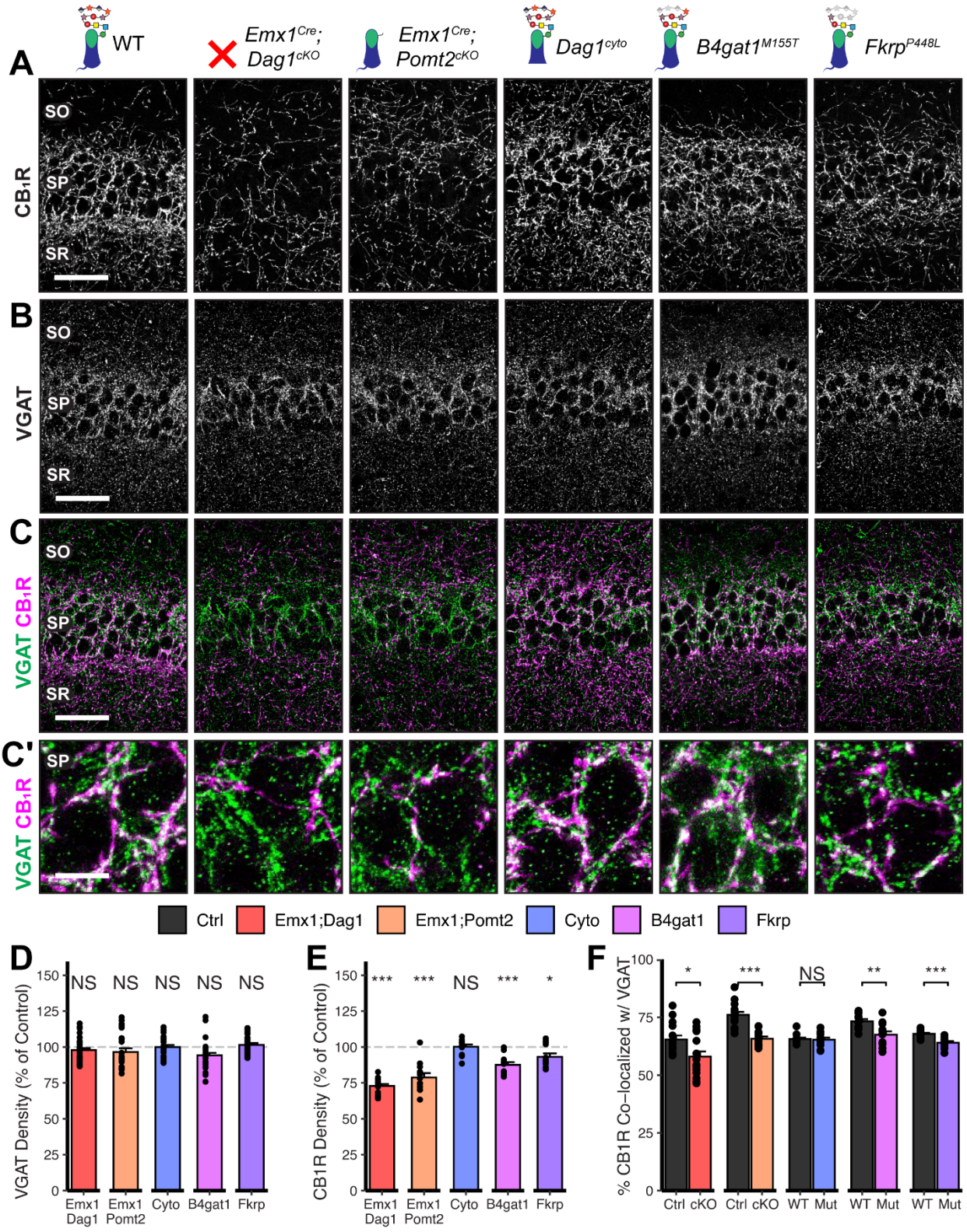

Figure 5. *Dag1* and *Pomt2* cKOs exhibit impaired CB1R⁺ basket synapse formation in *stratum pyramidale* of hippocampal CA1. P30 coronal sections

immunostained for **(A)** CB_1R and **(B)** VGAT in hippocampal CA1; merged image in **(C)** shows CB_1R in magenta and VGAT in green. (A-C) Scale bar = 50µm. (Higher magnification view of SP in **(C')**; scale bar = 10µm.) **(D)** Quantification of VGAT puncta density in SP expressed as a percent of control. **(E)** Quantification of CB_1R puncta density in SP expressed as a percent of control. **(F)** Quantification of co-localization between VGAT and CB_1R in SP to estimate putative CB_1R^+ basket cell synapse formation. Error bars show mean + SEM. (For quantification of puncta densities and co-localization in SO and SR see **Fig. 5 Supp. 1**.) See **Supplementary Table 1** for Ns. *Significance: * = $p < 0.05$, ** = $p < 0.01$, *** = $p < 0.001$, NS = $p \geq 0.05$. Abbreviations: SO, stratum oriens; SP, stratum pyramidale; SR, stratum radiatum.*

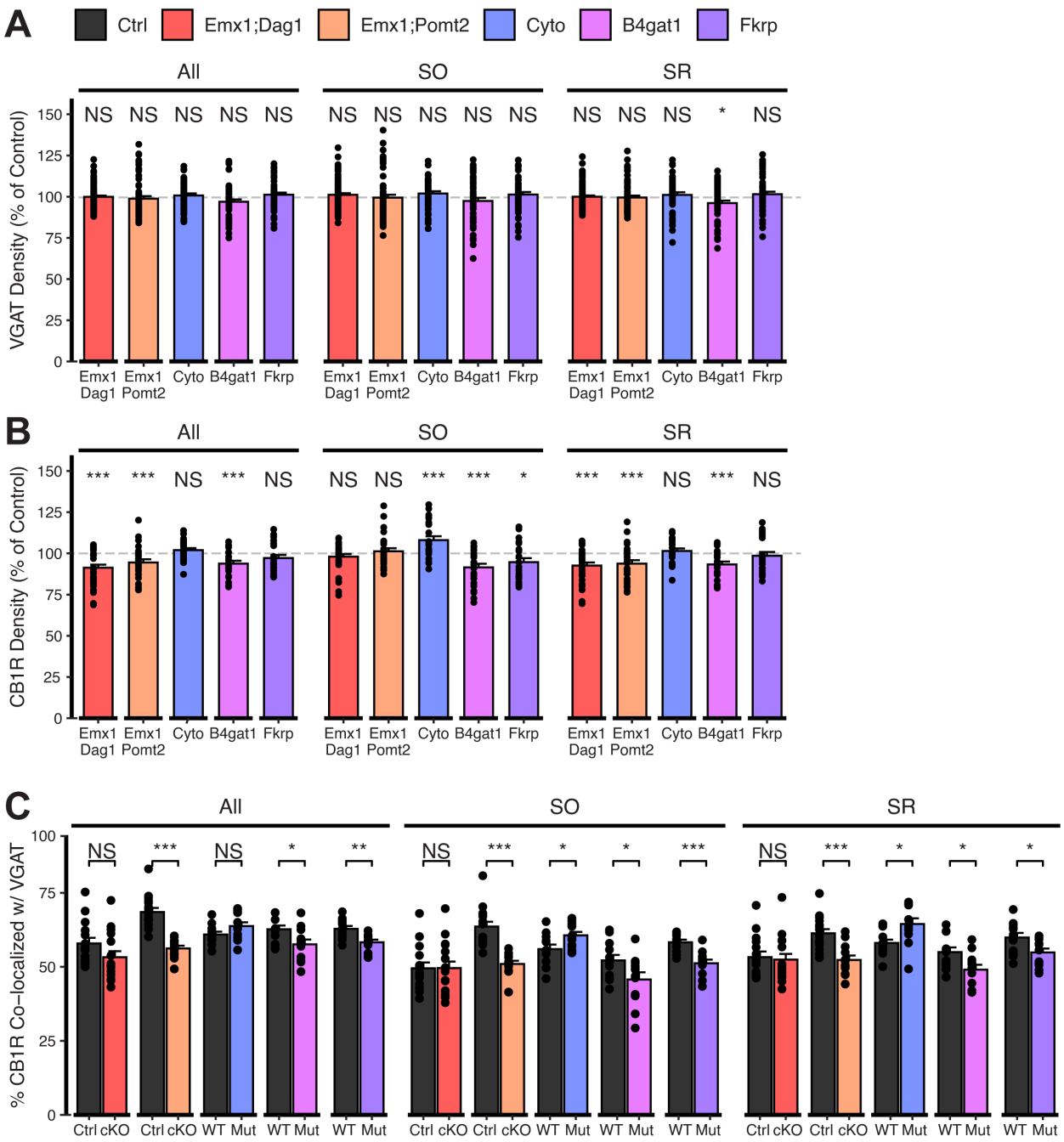

Figure 5 Supplement 1. Extended quantification of images in Figure 5A-C. Quantification within hippocampal CA1 SO and SR regions and all regions pooled together. **(A)** Quantification of VGAT puncta density expressed as a percent of control. **(B)** Quantification of CB_1R puncta density expressed as a percent of control. **(C)** Quantification of co-localization between VGAT and CB_1R to estimate putative CB_1R^+ basket cell synapse formation. Error bars show mean + SEM. (To see quantification of puncta densities and co-localization in SP see **Fig. 5D-F**.) See **Supplementary Table 1**

for Ns. *Significance: * = $p < 0.05$, ** = $p < 0.01$, *** = $p < 0.001$, NS = $p \geq 0.05$. Abbreviations: SO, stratum oriens; SP, stratum pyramidale; SR, stratum radiatum.*

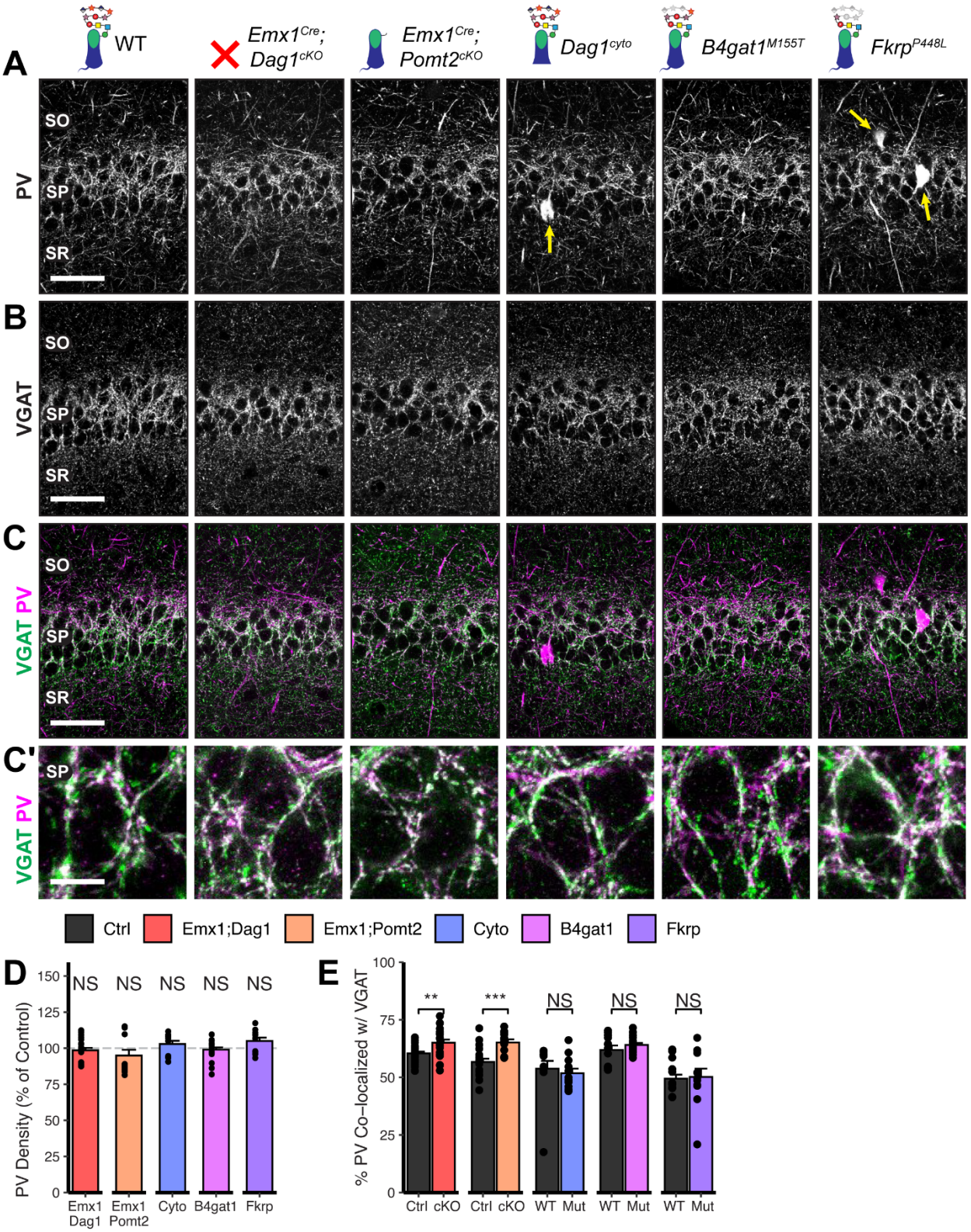

Figure 5 Supplement 2. *Dag1* and *Pomt2* cKOs exhibit increased PV⁺ basket synapse formation in *stratum pyramidale* of hippocampal CA1. P30 coronal sections immunostained for **(A)** PV and **(B)** VGAT in hippocampal CA1; merged image

in **(C)** shows PV in magenta and VGAT in green. Yellow arrows indicate PV^+ interneuron cell bodies. (A-C) Scale bar = 50µm. (Higher magnification view of SP in **(C')**; scale bar = 10µm.) **(D)** Quantification of PV puncta density in SP expressed as a percent of control. **(E)** Quantification of co-localization between VGAT and PV in SP to estimate putative PV^+ basket synapse formation. Error bars show mean + SEM. (To see quantification of puncta densities and co-localization in SO and SR see **Fig. 5 Supp. 2**.) See **Supplementary Table 1** for Ns. *Significance: * = $p < 0.05$, ** = $p < 0.01$, *** = $p < 0.001$, NS = $p \geq 0.05$. Abbreviations: PV, parvalbumin; SO, stratum oriens; SP, stratum pyramidale; SR, stratum radiatum.*

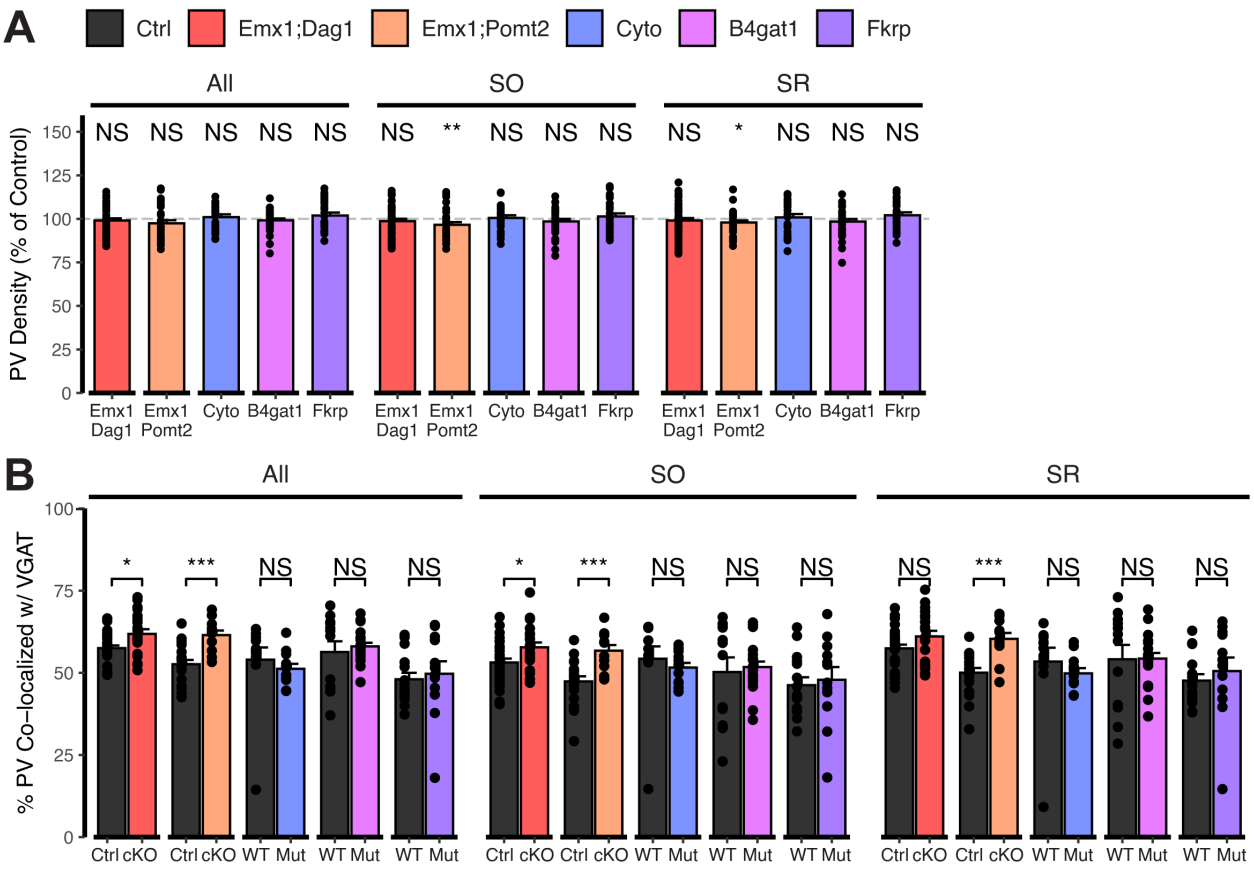

Figure 5 Supplement 3. Extended quantification of images in Fig. 5 Supp. 2A-C. Quantification within hippocampal CA1 SO and SR regions and all regions pooled together. **(A)** Quantification of PV puncta density expressed as a percent of control. **(B)** Quantification of co-localization between VGAT and PV to estimate putative PV$^+$ basket cell synapse formation. Error bars show mean + SEM. (To see quantification of puncta densities and co-localization in SP see **Fig. 5 Supp. 2D-E**.) See **Supplementary Table 1** for Ns. *Significance: * = p < 0.05, ** = p < 0.01, *** = p < 0.001, NS = p ≥ 0.05. Abbreviations: PV, parvalbumin; SO, stratum oriens; SP, stratum pyramidale; SR, stratum radiatum.*

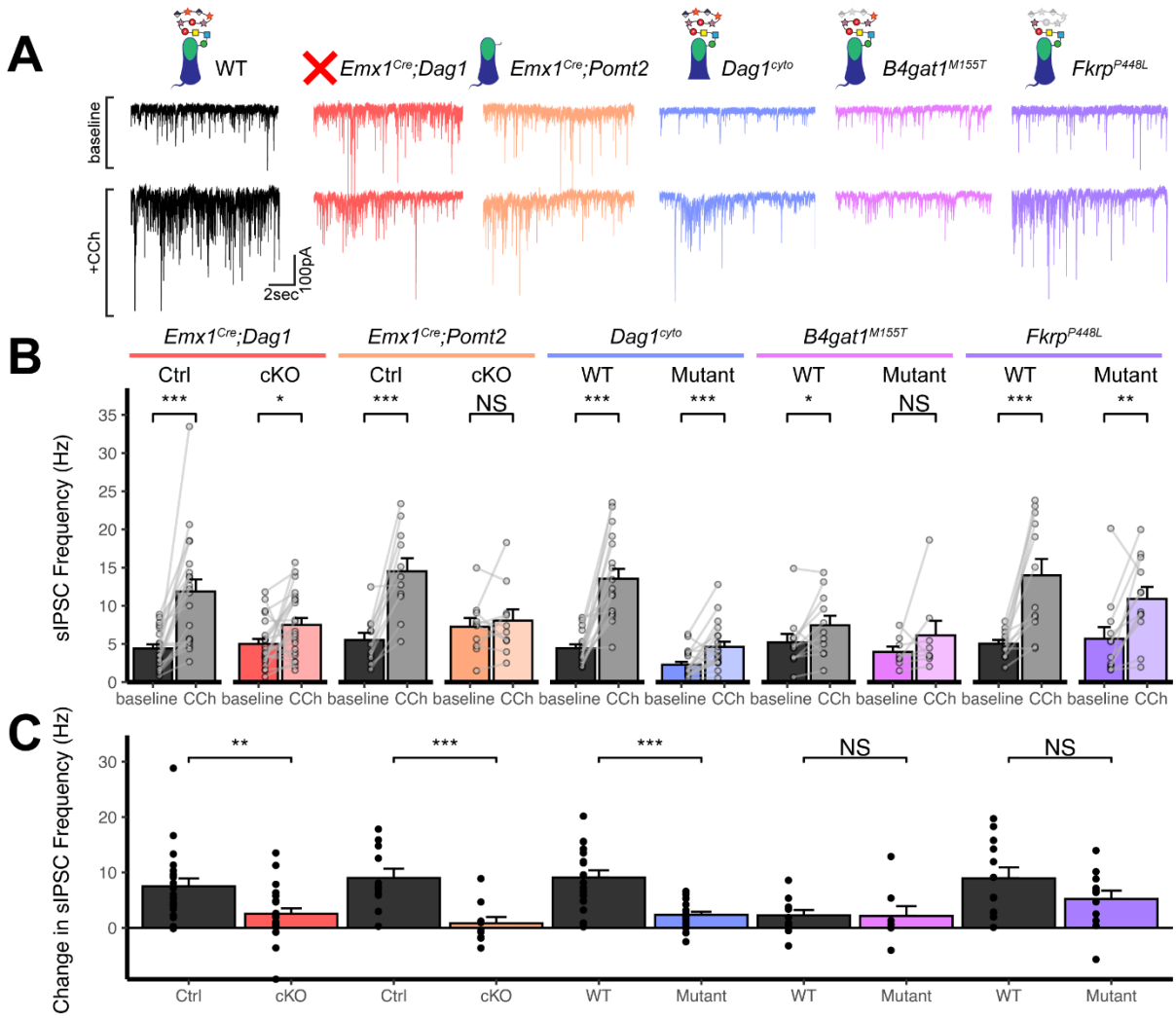

Figure 6. *Dag1* is required for CCK⁺/CB₁R⁺ IN synapse function in hippocampal CA1 in a manner dependent on both glycosylation and intracellular interactions. **(A)** Representative traces showing 15 seconds of sIPSC recordings at baseline (top) and after the addition of carbachol (bottom). **(B)** Quantification of average sIPSC frequency at baseline and after the addition of carbachol. **(C)** Quantification of the change in sIPSC frequency with the addition of carbachol. Error bars show mean + SEM. See **Supplementary Table 1** for Ns. *Significance: * = $p < 0.05$, ** = $p < 0.01$, *** = $p < 0.001$, NS = $p \geq 0.05$. Abbreviations: sIPSC, spontaneous inhibitory postsynaptic current; CCh, carbachol.*

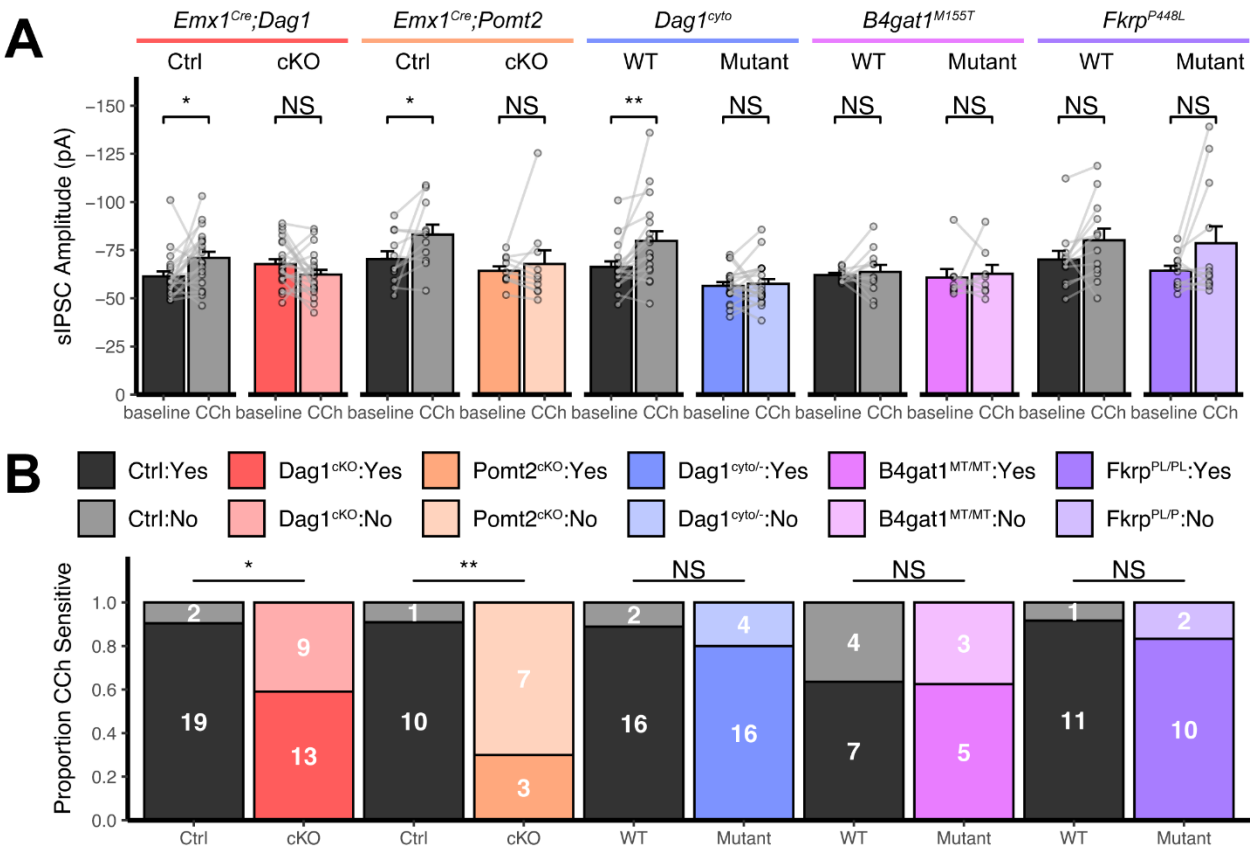

Figure 6 Supplement 1. Additional quantification of sIPSC recordings. (A) Quantification of average sIPSC amplitude at baseline and after the addition of carbachol. Error bars show mean + SEM. **(B)** Quantification of the proportion of carbachol-sensitive cells within each genotype. Non-responsive cells are shown in lighter color, responsive cells are shown in darker color. See **Supplementary Table 1** for Ns. *Significance: * = p < 0.05, ** = p < 0.01, *** = p < 0.001, NS = p ≥ 0.05. Abbreviations: sIPSC, spontaneous inhibitory postsynaptic current; CCh, carbachol.*

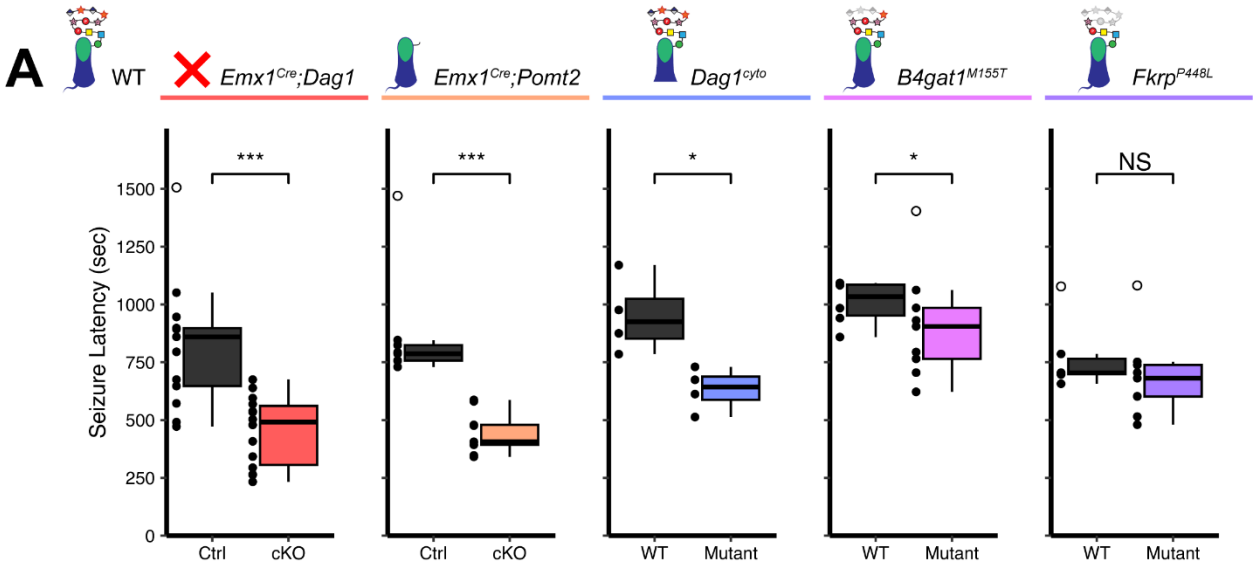

Figure 7. Reduced seizure induction threshold in models of dystroglycanopathy. (A) Quantification of latency (in seconds) to generalized tonic clonic seizure upon exposure to 10% flurothyl delivered at a constant rate. Open points denote statistical outliers. See **Supplementary Table 1** for Ns. *Significance: * = $p < 0.05$, ** = $p < 0.01$, *** = $p < 0.001$, NS = $p \geq 0.05$.*

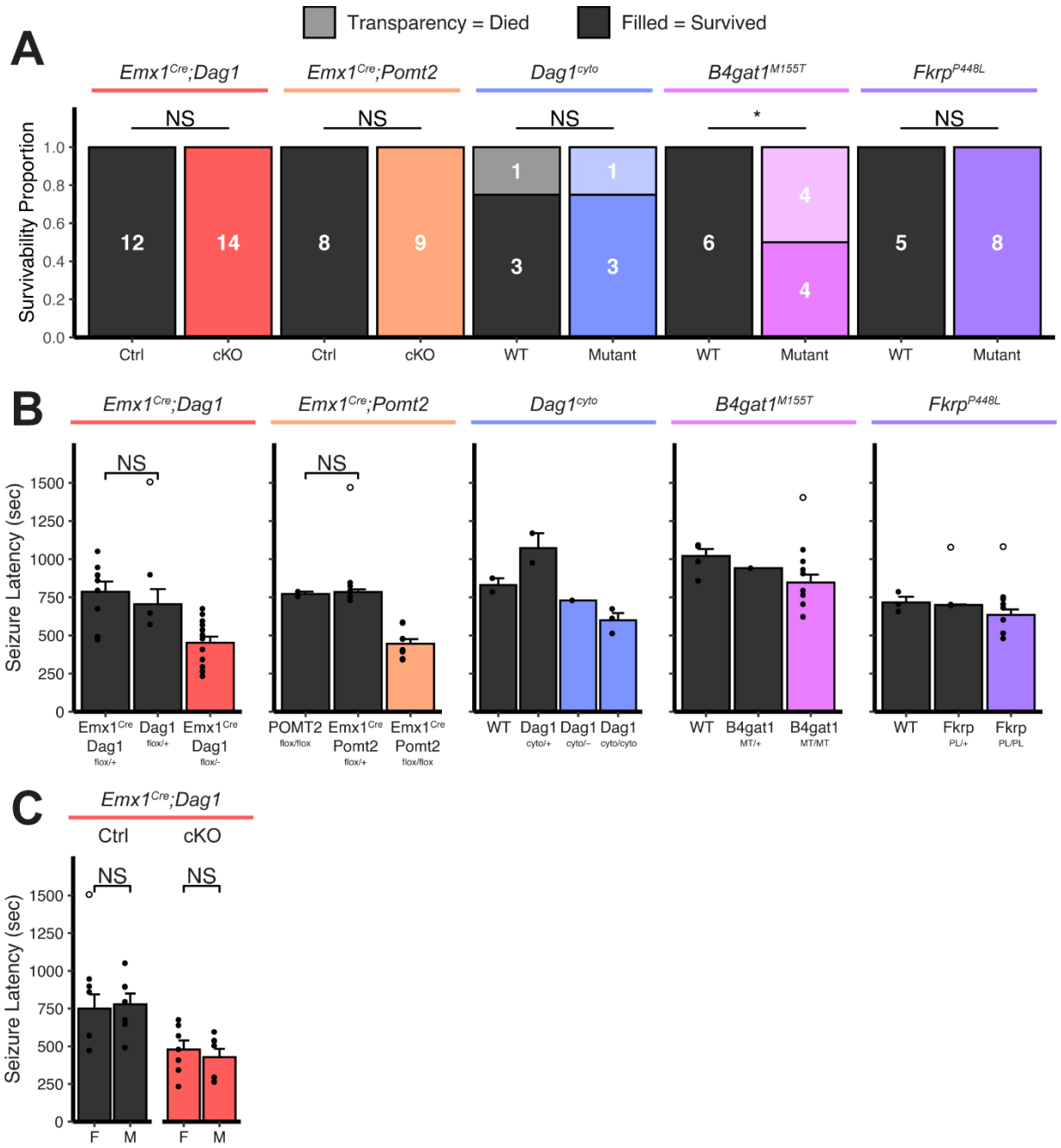

Figure 7 Supplement 1. Extended seizure induction threshold data.
(A) Proportion of mice that died as a direct result of a flurothyl-induced seizure. Survivors are depicted in darker colors, fatalities in lighter colors. **(B)** To minimize the number of animals needed for this experiment, certain genotypes were pooled together. Here we show that pooled genotypes are not different. Statistical tests were run where Ns were sufficient to provide meaningful comparison. **(C)** Seizure latencies split by sex. Note: only the *Emx1^{Cre};Dag1* group is powered sufficiently to statistically compare sexes. Open points denote statistical outliers. Error bars show mean + SEM.